Sedimentary architecture of a prograding oolitic-siliciclastic wedge: response to changes in wave-base oscillation (Kimmeridgian, Iberian Basin)

Jorge Val*, Beatriz Bádenas & Marcos Aurell

Dpto. Ciencias de la Tierra, Universidad de Zaragoza, 50009 Zaragoza, Spain

*Corresponding author, email address: jorgevalmunoz@gmail.com (Jorge Val)

ABSTRACT

A detailed facies and sequential architectural analysis has been carried out along the wedge-shaped shallow marine cross-bedded oolitic-siliciclastic Ricla Member (Kimmeridgian, Northern Iberian Basin). The obtained results are based on fieldwork along the 4x1 km continuous outcrops with the use of high-resolution photomosaics and drone-made videos, which have led to a precise and extensive facies reconstruction. Three main facies that are laterally related (A to B to C) in down-dip direction have been differentiated, which correspond to the topset, foreset and bottomset parts of a sloping depositional surface. Sedimentation was controlled by sweeping drift and downwelling storm-induced currents causing avalanching processes, with the deep action of oscillatory currents. The sedimentary architecture consists in 5 successive units composed by several sub-units, arranged according to different stacking patterns, which reflect the sedimentary response to wave-base oscillations superimposed to the regressive part of a third-order transgressive-regressive cycle. The sedimentological features indicate that this unit, which has been

25 previously interpreted as a dune complex fit with an infralittoral prograding wedge
26 model, as it is observed in geographically close and stratigraphically similar units. The
27 Ricla Member is therefore regarded as an example of a well-exposed grain-supported
28 unit with broad potential application to other prograding grain-dominated lithosomes
29 that do not conform to the traditional sand shoal model.
30
31 ***Key-words:*** Infralittoral prograding wedge, oolitic, siliciclastic, high-frequency
32 cycles, facies architecture, Kimmeridgian
33
34 **1. Introduction**

35 Reconstructing the sedimentary architecture and facies heterogeneities from the
36 analysis of well-exposed grain-supported prograding units provides valuable
37 information for comparison with subsurface analogous hydrocarbon reservoirs. Upper
38 Jurassic outcropping analogues are of particular interest to further understand
39 significant hydrocarbon reservoirs, such as those found in the Smackover Formation in
40 the USA Gulf Coast or the Arab-D Formation in Arabia (e.g., Benson, 1988; Grötsch *et*
41 *al*., 2003, San Miguel *et al*., 2013). Detailed outcrop analysis is required to achieve
42 precise understanding about the sedimentary architecture of prograding units.
43 Recognition of new stratigraphic details can improve the interpretation of carbonate
44 lithosomes and may trigger new exploration opportunities in reservoirs, promoting
45 more realistic models for characterization of inter-well heterogeneities (Pomar et al.,
46 2015). In particular, Kleipool *et al*. (2015, 2016) remark the potential use of the well-
47 exposed Kimmeridgian (Upper Jurassic) mixed oolitic-siliciclastic sand complex of Ricla

Member (Iberian Basin, NE Spain) studied in the present work, as a reference analogue for reservoirs developed in prograding carbonate ramps.

The architecture and facies distribution on sedimentary units is related to the sedimentary processes as well as to their response to sea-level fluctuations and tectonics (e.g., Schlager, 2005). Sediment production and distribution by hydrodynamic factors are essential sedimentary processes in carbonate ramps. Carbonate sand-shoal deposits are usually found in epeiric platforms and shallow domains of carbonate ramps, located around or above wave base level (e.g. Tucker, 1985; Tucker & Wright, 1990). Sand-sized deposits can also form significant accumulations characterized by the basinward progradation in subtidal domains located below wave base forming infralittoral prograding wedges (e.g. Pomar & Tropeano, 2001; Lobo *et al*., 2004; Fernandez-Salas *et al*., 2009; Pomar *et al*., 2015; Andrieu *et al.*, 2017). These sand bodies are the result of avalanching processes below the wave base level of sediment swept seaward from the shallow domains by the combined effect of storm-generated longshore and downwelling currents (Hernandez-Molina *et al*., 2000).

The Ricla Member (Iberian Basin, NE Spain) is an outstanding example of a prograding oolitic-siliciclastic sand complex developed around wave-base in the shallow areas of the Kimmeridgian carbonate ramp (Bádenas & Aurell, 2001a). This unit is exposed in different dip to strike-oriented sections along a 6 km long transect, forming a wedge-shaped unit, up to 22 m-thick in the most proximal (northern) outcrop area and pinching out basinward (to the south), down to 5 m-thick on distal localities. The 6 km-long continuous exposures with nearly undeformed and uncovered clear panoramic outcrops, allow studying the facies heterogeneities and lateral and vertical distribution of this cross-bedded oolitic-siliciclastic sand complex.

72 The proposed aims of this work are the following: (1) to get a precise facies
73 reconstruction of the Ricla oolitic-siliciclastic sand-wedge complex and its
74 heterogeneities, across a selected 4 x 1 km (down-dip to strike) square area; (2) to
75 understand how those sedimentary facies are inter-related and arranged into
76 architectural elements along the whole sedimentary unit; (3) to complete and improve
77 the knowledge of the depositional mechanisms controlling the architecture of the
78 prograding sand-wedge complex in a regressive context, and in particular the effect of
79 the high-frequency wave-base oscillations in the resultant sedimentary architecture.
80

81 **2. Geological setting**

82 The dominant greenhouse climate conditions during the Jurassic, and its associated
83 high sea-level, caused the flooding of wide continental areas, giving rise to shallow
84 epeiric seas in Western Europe (Jenkyns, 1996). That was the case of the Iberian Basin,
85 where extensive carbonate ramps were developed during the Jurassic (Fig. 1A). The
86 development of carbonate ramps is usually linked to those platforms in which the
87 sedimentary rates are similar for shallow and deeper domains, favouring the
88 construction of the ramp geometry instead of distal slope platform or barrier platform
89 morphology (Wright & Faulkner, 1990). However, the shallow ramp developed in the
90 Iberian Basin at around 20-25º N palaeolatitude (Osete *et al.*, 2011) during
91 Kimmeridgian (Fig. 1A) is a remarkable example in which the gently inclined geometry
92 is kept up in spite of differential carbonate production rates. The production was
93 dominantly located in the shallow areas, mainly controlled by phototrophic organisms
94 (coral patch reefs) and ooid generation. The lack of significant deeper production was
95 compensated by an important offshore transport associated to storm return currents,

96 which reworked a significant bulk of sediment from the high productivity shallow areas
97 to the deeper domains and balanced its sedimentary rates (Aurell *et al*., 1998; Bádenas
98 & Aurell, 2001a). The effect of tides and fair-weather waves was probably limited in
99 the shallow area of the ramp due to the dissipation of its energy along its wide
100 extension (Tucker & Wright, 1990), but the absence of protective barriers determined
101 the susceptibility to the action of storms and hurricanes (Aigner, 1985), so deposition
102 was mainly dominated by the return currents associated to storms and hurricanes
103 (Bádenas & Aurell, 2008).

104 The Jurassic outcrops located north of Ricla (Iberian Range, NE Spain) expose the
105 proximal areas of the low-angle Kimmeridgian ramp. The shallow-water oolitic-
106 siliciclastic Ricla Member studied here was developed in the northern Iberian Basin,
107 south of the Ebro Massif (Fig. 1B), and facing both hurricanes pathways and winter
108 storms (Marsaglia & Klein, 1983; Price *et al*., 1995; Bádenas & Aurell, 2001b).

109 The Kimmeridgian stratigraphic succession in the northern Iberian Basin (Fig. 1C)
110 comprises two transgressive-regressive (third-order) Kim-1 and Kim-2 sequences
111 (Bádenas & Aurell, 2001a; Aurell *et al*., 2003). The Kim-1 sequence is mostly early
112 Kimmeridgian in age. In the Ricla outcrops, the transgressive and lower regressive part
113 of the Kim-1 sequence is represented by a marl-dominated succession (Sot de Chera
114 Formation) grading upwards into the well-bedded burrowed sandy limestones of the
115 lower Loriguilla Formation, interpreted as outer to middle ramp deposits. The upper
116 regressive stage of the Kim-1 sequence is represented by the sudden progradation of
117 the mid ramp Ricla oolitic-siliciclastic Member occurring around the lower–upper
118 Kimmeridgian boundary (Bádenas & Aurell, 2001a). This assignment is supported by
119 the new finding of *Crussoliceras* sp. (lower Kimmeridgian, *divisum* Zone) in a burrowed

sandy limestone level located c. 10 m below the studied Ricla Member. The Ricla Member is bounded on top by a sharp sedimentary discontinuity that corresponds to the boundary between the Kim-1 and Kim-2 sequences. This discontinuity is a cemented and ferruginous flat surface with occasional borings, without evidence for subaerial exposure (Bádenas and Aurell, 2001a). Above this discontinuity a major deepening event at the onset of the deposition of the Kim-2 sequence resulted in the formation of a condensed limestone level rich in poorly sorted irregular oncoids and varied skeletal grains including corals, which can be traced all across the Ricla outcrop. This condensed oncolitic-rich level is in turn overlain by middle ramp coralline limestones grading distally to lime mudstone dominated successions (i.e., Torrecilla and upper Loriguilla formations, respectively; Bádenas *et al*.,2005).

Previous analysis of the Ricla Member by Bádenas & Aurell (2001a) showed the overall lithofacies distribution and the sedimentary architecture within this oolitic-siliciclastic sand-wedge complex (Fig. 1D). The reconstruction of the sedimentary architecture of the Ricla Member is improved here by the detailed analysis of a 4x1 km outcropping area located in the northern and thicker part of the Ricla Member. In general terms, these deposits are characterized by an initial shallowing-upward stage of prograding siliciclastic lobes and channels, represented by cross-bedded and channelled oolitic-bioclastic sandstones and micro-conglomeratic beds at its lowermost part (Fig. 1D). Above these levels, there was a sharp progradation of large-scale foreset oolitic-sandy grainstones passing down-dip to sandy-oolitic and skeletal grainstones (Bádenas & Aurell, 2001a).The basal cross-bedded and channelled oolitic-bioclastic sandstones have been used as a datum in the present work (called here basal unit).

3. Methods

The exceptional outcrop conditions of the Kimmeridgian succession in the Ricla area have allowed carrying out a widespread fieldwork and the physical tracing along the whole sand-wedge Ricla Member to get sedimentological data and to identify their architectural elements.

The whole 4x1 km outcropping area selected is located in the northern part of the Ricla outcrops, and has been divided into 10 panoramic outcrop views, which are 200 m to 660 m in length (Fig. 2A). Outcrops 1 to 6 are located successively, from the proximal (north) to the distal (south) areas, and are nearly down-dip oriented regarding to the ramp slope. Outcrops 7 to 10 are perpendicular to the outcrops 1 to 6, and therefore they are oblique and strike oriented with respect to the ramp slope. Fieldwork has been supplemented by detailed study using high-resolution continuous photomosaics and drone-made videos on those selected panoramic outcrops in order to accurately map and delimit facies and architectural elements (master bedding surfaces and sedimentary units), getting a precise analysis of geometries in a 3D reconstruction. In addition, palaeocurrents and minimum lateral extension of each sedimentary unit have been measured to characterize the setting-up patterns for each successive building stage and the variations in migration trends.

The identification of facies has been accomplished on the basis of the bedding patterns and the presence of different types of sedimentary structures, characterizing depositional features. The textural characteristics have not been used as a key criterion for facies differentiation. Nevertheless, the petrographic analysis of rock samples in polished slabs and thin sections has allowed identifying different lithofacies

168 attending to the texture and components (mainly siliciclastic and carbonate grains),
169 and these aspects have been taken into account for the reconstruction of the
170 sedimentary model. Bioturbation intensity has been characterized using the
171 bioturbation index (BI) defined by Taylor & Goldring (1993).
172
173 **4. Results**
174 *4.1. Facies types*
175 The sedimentological analysis in the Ricla area has allowed identifying a set of
176 facies types on the basis of bedding patterns and sedimentary structures. Three main
177 facies that are laterally related (A to B to C) in down-dip direction have been
178 differentiated and mapped along the selected outcrops (Fig. 2B). There is also an
179 occasional facies D occurring in the northern sector (see outcrop 1 in Fig. 2B).
180 Facies A is mainly composed by dm- to m-thick tabular beds including dm-thick sets
181 of bidirectional planar cross-stratification (Fig. 3A; see palaeocurrent data in section
182 4.2). Set boundaries are flat erosive surfaces, dipping less than 1-3˚. Bioturbation is low
183 and locally present on beds tops (BI: 0-1), including *Asterosoma* traces.
184 Facies B comprises 0.5 to 4 m-thick sets of planar cross-stratification with sigmoidal
185 to wedge geometry (Fig. 3B). Individual sets include dm-thick foreset beds with
186 internal lamination parallel to foreset tops, which show unidirectional down-dip
187 10˚average inclinations. Set boundaries are either non-erosive or erosive surfaces with
188 similar or less inclination than foreset beds. Sets usually display an offlap stacking (i.e.
189 in down-dip direction) and high-angle cross-bedded foresets in proximal localities, give
190 way to less inclined beds that distally interconnect with facies C. Sparse escape traces
191 are present (BI: 0-1).

192 Facies C consists of dm-thick tabular beds with frequent hummocky cross
193 stratification (HCS, with decimetre to metre-scale wavelength; Fig. 3C) and
194 unidirectional (down-dip) planar cross-lamination. Beds of facies C distally wedge and
195 interfinger with muddier deposits, including lime mudstone levels and burrowed marls.
196 The bioturbation index is low to moderate (BI: 2-3). The identified trace fossils include
197 *Asterosoma*, *Diplocraterion*, *Planolites* and *Skolithos*.
198 Facies A, B and C do not have significant differences in lithofacies. They correspond
199 to grainstones with variable proportions of quartz grains and ooids, and occasional
200 bioclasts (echinoids, bivalves, gastropods, brachiopods, corals and serpulids). Textures
201 can vary between individual beds and even within beds, from oolitic grainstones (Fig.
202 4A), oolitic-sandy grainstones (Fig. 4B) to oolitic sandstones (Fig. 4C). The ooids are
203 spherical to slightly ovoidal and generally well sorted, with diameter usually ranging
204 from 0.5 mm to 1 mm. Quartz grains generally form the ooid nuclei, and the ooid
205 cortices have fine concentric fibrous-radial laminae or alternating fibrous-radial and
206 micritic laminae (i.e. type 3 and mixed type 1-3 of Strasser, 1986, respectively).
207 Cements are equigranular and probably recrystallized, without evidence of vadose
208 conditions. The siliciclastic fraction is composed by sub-angular, fine to medium sand-
209 sized quartz grains. In the southern area, sand-sized quartz grains and quartzite
210 pebbles are more frequent, and the dominant lithofacies are oolitic-sandy grainstones,
211 oolitic sandstones (Figs. 4D and 4E) and heterometric micro-conglomerates (Fig. 4F).
212 Facies D corresponds to a tabular level with basal erosive surface and diffuse
213 parallel lamination (Fig. 3D). It consists of poorly sorted sandstones to micro-
214 conglomerates composed by sub-angular coarse sand quartz grains and quartzite
215 pebbles, bioclasts (mainly oyster shells and echinoids) and lime mudstone rip-up clasts.

4.2. Facies architecture

The continuous exposure of the Ricla outcrops has allowed reconstructing the facies architecture within the sand-wedge prograding Ricla Member. According to facies stacking pattern, presence of sharp bounding surfaces and palaeocurrent average values, five successive prograding units have been identified here overlying the basal sand-dominated unit used as a datum (units 1-5, Figs. 2B and 5). Unit boundaries represent sharp discontinuity surfaces that can be traced across the outcrop. These units are composed by sub-units bounded by slightly oblique down-slope dipping sharp surfaces (Figs. 2B, 6 and 7).

Unit 1 is 8 m-thick in the northern sector (see outcrops 1 and 7–9, Fig. 2B) and suddenly wedges in down-dip direction (between outcrops 1 and 2, see also outcrop 9, Fig. 2B). This abrupt wedging allows delimiting the southern limit of the unit and its minimum lateral extent (around 700 m, Fig. 5). Unit 1 is mainly formed by oolitic-siliciclastic large-scale foreset beds (facies B) with southwest-directed palaeocurrents (average value of 200˚; Fig. 5) and minor proportion of dm-thick sets of cross-stratified facies A and tabular HCS facies C. The analysis of the facies distribution in outcrops 1 and 7–9 reflects a lateral A-B-C facies relationship in accordance with the palaeocurrent (southwest) direction (Figs. 2B and 6); in the northeast outcrops 7–9 the unit is formed by large-scale foreset facies B and discrete occurrence of sets of cross-stratified facies A on top, whereas towards the southwest (outcrop 1) the unit also includes a 2.5 m thick lowermost sub-unit composed of tabular HCS facies C (Fig. 2B and 6). The mapping of facies in outcrop 1 also reveals that the upper part of Unit 1 is formed by the offlap stacking of up to 4 m-thick and *ca.* 600 m-long sigmoidal sub-

240 units, composed of large-scale foreset facies B. This facies occasionally pass down-dip
241 to tabular HCS facies C or with downlap contact with the underlying lowermost sub-
242 unit composed by vertically stacked tabular beds of HCS facies C (Fig. 6).
243 Unit 2 is a sigmoidal unit vertically and laterally stacked over Unit 1 (Fig. 2B). In the
244 northern outcrops 1 and 7–8 it has homogeneous thickness of 10 m (Fig. 6). Towards
245 the southwest (outcrop 2) it sudden increases in thickness up to 17.5 m, downlapping
246 the underlying sharp wedging of Unit 1 and the basal (datum) unit (Fig. 7). Further
247 southwards it gradually wedges through outcrop 3, thus reflecting its southern limit
248 and its maximum lateral extension (at least 1700 m, Fig. 5). In the northern outcrops 1
249 and 7–8, the base of Unit 2 is marked by an extensive decimetric tabular level of micro-
250 conglomerates (facies D) covering the top of previous Unit 1 (Figs. 2B and 6). Unit 2 is
251 formed by cross-stratified facies A (with northeast-southwest bidirectional
252 palaeocurrents: Fig. 5), large-scale foreset facies B (with southwest to south migration,
253 average values of 190˚-200˚: Fig. 5) and tabular HCS facies C. The analysis of the facies
254 distribution clearly reflects the lateral A-B-C facies change towards the palaeocurrent
255 (southwest and south) direction, which can also be mapped at outcrop scale (Fig. 2B).
256 Accordingly, in northern outcrop 7, the unit is almost exclusively formed by tabular
257 cosets of cross-stratified facies A. Towards the south and southwest (outcrops 1 and 8–
258 10) the unit is formed by offlapping sub-units encompassing facies A, B and C, and
259 locally showing down-slope shingling configuration (e.g. outcrop 1 in Fig. 6). Further to
260 the south (outcrop 2, Fig. 7), Unit 2 has a downlap architecture and is exclusively
261 formed by successive (and progressively thinner) 400 m-long sub-units of cross-
262 stratified facies B arranged with down-slope shingling to offlap stacking (Fig. 7).

263 Unit 3 is an up to 17 m-thick and 1600 m-long sigmoidal unit that is stacked in
264 offlap respect to Unit 2 (see outcrops 2 to 5 in Fig. 2B). This unit is dominated by the
265 large-scale foreset facies B, with southeast palaeocurrents (average palaeocurrent
266 values of 160˚), which reflect an eastwards palaeocurrent deviation in comparison to
267 the previous units (Fig. 5). The unit is formed by successive 700 m-long sub-units with
268 offlap arrangement formed by facies A (see outcrops 2 and 3, Fig 2B), passing down-
269 dip to large-scale foreset facies B and distally to tabular HCS facies C with interbedded
270 marls and lime mudstone beds (see lower part of the outcrops 4 and 5, Fig. 2B).
271 Units 4 and 5 are two sigmoidal units stacked in offlap and downstepping
272 architecture, with reduced thickness compared to the previous units. Unit 4
273 progressively thins southwards from 9 m in outcrop 5 down to 4 m in outcrop 6 (Fig.
274 2B). Its basal boundary with Unit 3 is erosive, as it is reflected by the presence at the
275 lowermost part of Unit 4 of a lenticular conglomeratic deposit including lime mudstone
276 intraclasts, derived from the erosion of muddy facies of Unit 3 (see outcrop 5 in Fig.
277 2B). Unit 5 thickens progressively through outcrop 6 up to 4.5 m-thick to the south (Fig.
278 2B). Both units are mainly formed by low-angle offlapping to downstepping sub-units
279 of facies B with southeast palaeocurrents (average values of 120˚-130˚, Fig. 5), and
280 local presence of bidirectional cross-stratified facies A. Both units have lower oolitic-
281 dominated sub-units and upper siliciclastic-dominated sub-units (Fig. 8). The bounding
282 surfaces of sub-units are usually burrowed and encrusted.
283
284 **5. Significance of the facies types**
285 The stacking of laterally-related A, B and C facies observed here (Fig. 9A) at unit
286 and sub-unit scale represent the successive depositional parts around and within a

287 sloping depositional surface in which topset, foreset and bottomset parts have been
288 identified (Fig. 9B). This kind of sedimentary architecture is widely known as clinoform
289 in the sense of Mitchum (1977), after Rich (1951) who firstly defined this term for the
290 inclined strata surfaces (i.e. the foreset itself).

291 Topset facies A is characterized by dm-thick sets of planar cross-stratification with
292 bidirectional palaeocurrents. The horizontal geometry or slight down-slope inclination
293 of the surfaces bounding the sets (<3˚: Fig. 9A)suggest deposition in a flat topography
294 to low-angle sea-bottom located inshore of the high-angle slope of the clinothem
295 represented by the accumulation of large-scale foreset facies B. Comparison of
296 palaeocurrent direction of facies A and its down-dip related foreset facies B (e.g. Unit
297 2, Fig. 5), reflects that direction of the small-scale bedforms found in facies A was
298 oblique to the prograding migration of facies B. Facies A has been assigned to the
299 influence of sweeping and longshore drift in the lower shoreface area, caused by
300 feeder currents of the rip circuit induced by the incidence of storms and its return
301 flows. The observed bidirectional nature of these longshore currents can be explained
302 by the variation of the impact point and incidence angle of the storm-induced currents
303 (Bowman *et* al., 1992; MacMahan *et al*., 2006; Castelle *et al*., 2016). An alternative
304 explanation of tide-induced currents controlling bedform migration cannot be ruled
305 out. However, evidences for tidal influence in the interior shallow domain of the
306 Kimmeridgian epeiric platform are scarce (e.g., Aurell *et al*., 1998; Bádenas and Aurell,
307 2001a).

308 Foreset facies B records the unidirectional basinwards migration, which has been
309 previously related to the action of episodic storm-induced return flows (Bádenas &
310 Aurell, 2001a). Further analysis carried out in this work indicates that large-scale

311 foreset facies B correspond to the down-slope avalanching accumulation along a
312 slightly inclined surface below the mean wave base, controlled by the sweeping action
313 of storm-induced downwelling currents (Fig. 9B, C). The growth of this deposit was
314 intermittent, and accretion stages alternated with non-sedimentation and even
315 erosion, as it is indicated by different sets characterized by parallel foreset beds and
316 separated by oblique sharp interruption surfaces (erosive and non-erosive set
317 boundaries). Erosive set boundaries cut the previous cross-strata and are likely to be
318 generated by higher energy events (similar to that observed in tidal dunes by Olariu *et*
319 *al*., 2012). Non-erosive set boundaries are parallel to the previous cross-strata, and
320 posterior cross-strata are arranged concordant over the surface, thus reflecting
321 episodes of non-sedimentation and reactivation. Therefore, the dip angle of foresets
322 varies throughout deposition (around a mean of 10˚) as the successive avalanching
323 and/or erosional stages controlled by the wave oscillations, define the topography for
324 next avalanching deposits.
325 Bottomset tabular facies C indicate a nearly flat topography at the toe of the
326 clinoform. The cross-laminated structures with unidirectional palaeocurrents represent
327 the migration of small-scale bedforms induced by the bottomset currents distally to
328 the foreset slope. Presence of hummocky cross stratification also records the
329 occasional reworking by oscillatory flows induced by exceptional storms, as observed
330 in modern analogues (Hernández-Molina et al., 2000). The interfingered marly and
331 lime mudstone deposits reflect alternating periods of agitation and quiescence with
332 lime mud settling from suspension.
333 The lateral relation between topset and foreset parts is usually convex-shaped,
334 while the union between foreset and bottomset parts shows a concave-shaped dip

angle reduction, as commonly observed in clinoformed depositional models (Steel & Olsen, 2002).

As regards to the lithofacies and texture of facies A, B and C, the presence of fibrous-radial ooids indicates high-energy shallow domains with normal salinity (Strasser, 1986). Thus, ooids generation could be settled in the inner topset domain as well as in more proximal areas affected by wave action or even tidal influence, from where ooids would be mobilized, as observed in modern analogues of Bahamas tide-dominated shoals and wave-dominated systems (Rankey & Reeder, 2011; Rankey, 2014). The alternation of ooid-dominated to siliciclastic-dominated lithofacies even at bed scale would most likely record variations in the terrigenous sediment supply and heterolithic segregation, such as observed in other mixed deposits alternating carbonate and siliciclastic fractions (Chiarella & Longhitano, 2012). There is not enough evidence to solve if siliciclastics were brought into the system by littoral drift or direct fluvial input. Nevertheless, sub-angular quartz grains in the ooid nuclei and in the siliciclastic fraction indicate reduced reworking and the proximity of the continental source-area, probably from the Ebro Massif located northwards to the study area (Bádenas & Aurell, 2001b).

Facies D, locally recorded at the base of Unit 2 in the northern sector (Fig. 2B) is unrelated with the lateral relationship between the facies A, B and C. Bad sorting, reduced thickness, heterogeneous nature of siliciclastic to carbonate grains (skeletal grains, intraclasts) and the sharp erosive base indicate that this facies correspond to a lag deposit. This deposit could be a tempestite deposit at the toe of the bottomset originated by an exceptional storm event (Myrow & Southard, 1996) or related to the

358 transgressive event developed over a ravinement erosion surface from dynamic
359 condensation (Swift, 1968; Allen & Posamentier, 1999; Cattaneo & Steel, 2003).
360
361 **6. Discussion**
362 *6.1. Facies architecture: response to wave-base oscillations*
363 The architecture of shallow marine prograding units results from the integrated
364 relationship between accommodation changes, sediment supply, hydrodynamics and
365 previous topography (Driscoll & Karner, 1999; Puig *et al*., 2007). The detailed analysis
366 of the facies distribution performed in the Ricla Member reveals a complex internal
367 architecture of facies and, thus, of hydrodynamic processes and physical
368 accommodation controlling the sedimentary evolution.
369 The overall sedimentary architecture of the Ricla Member reflects that
370 accommodation space was largely exceeded by sediment supply, causing the
371 basinwards migration of deposition, which generated a gentle sloping surface (Walsh
372 *et al*., 2004). The Ricla Member as a whole corresponds to a sand-wedge deposit
373 developed in a long-term regressive context, as the dominant prograding and
374 offlapping geometries indicate (Bádenas and Aurell, 2001a). In addition, in order to
375 explain the internal architecture of the Ricla Member is necessary to invoke the
376 presence of a higher-order oscillatory signal superimposed to this long-term regressive
377 trend (Fig. 10). Sedimentary evolution and stacking patterns of different units within
378 this sand-wedge reflects the alternation of accumulation processes together with
379 episodes of erosion caused by different nature factors. Foreset surfaces and set
380 boundaries can be considered as autogenic, as they reflect accretional and erosional
381 stages due to variations in the energetic conditions, while successive sub-unit and unit

boundaries would indicate allogenic changes in the equilibrium profile of the wave-base. The storm-controlled nature of this depositional model would determine a strong dependency on the frequency and intensity of storms, affecting the rate between deposition and erosion. Therefore, variations in the available accommodation space would be controlled by wave-base oscillations driven by the short-term climate variation (Hampson & Storms, 2003; Storms & Hampson, 2005). So, each one of the 5 recognized units reflect the sedimentary response of the depositional system to wave-base oscillations superimposed to the regressive stage of the third-order Kim-1 sequence (Hunt & Tucker, 1992, 1995; Aurell *et al.*, 1998). These oscillations could be probably driven with climate controlled fourth- or fifth-order sea-level variations, although the absence of precise chronostratigraphic data does not allow a reliable age calibration.

Unit 1 represents a rapid lateral accretion of the prograding wedge during a still-stand wave-base stage, as indicated by the offlaping geometry of the successive sub-units (see outcrops 1 and 7-9).In addition, outcrop 1 includes a lower sub-unit composed by vertically stacked tabular beds of HCS facies C, which would reflect and initial stage of rapid creation of accommodation previous to the facies B progradation, favouring the setting of relatively deep depositional conditions compared with the underlaying sand-dominated deposits (i.e. basal unit).

Unit 2 records at its lower part an initial stage of creation of accommodation that allowed its vertical stacking over Unit 1. The widespread presence at the lowermost part of Unit 2 of the conglomeratic deposit which can be interpreted as a transgressive lag (i.e., Facies D), gives support to the existence of this initial sea-level rise event, which caused subaqueous erosion and reworking (Allen & Posamentier, 1999;

406 Cattaneo & Steel, 2003). This initial stage of accommodation gain was lately
407 compensated by the sediment supply, as it is indicated by the overall prograding offlap
408 geometries observed in most of Unit 2. The extensive down-slope shingling stacked
409 sub-unit in the top of outcrop 1 marks the highest position reached by the wave-base
410 according to the sedimentary record of this unit, and it is followed by a still-stand stage
411 represented by the offlap stacked sub-units in outcrop 2.

412 The offlap stacking of the Unit 3 and its prograding sub-units indicates a stage of
413 still-stand wave-base. However, at the end of the deposition of Unit 3 there are
414 evidences of accommodation loss and even submarine erosion, which are most likely
415 related to a stage of a high-frequency sea-level fall and related lowering of the wave
416 base. Accordingly, the wave-base reached the sea floor, causing widespread erosion
417 and generation of intraclasts that were eventually incorporated in the lowermost
418 levels of the overlying Unit 4. In particular, at the lower part of Unit 4 there is a
419 lenticular conglomeratic deposit with abundant intraclasts (see section 4.2), which was
420 probably caused by an extraordinary storm event. The presence of this lenticular
421 deposit reinforces the interpretation of wave-base falling after Unit 3 deposition.

422 The overall geometry of units 4 and 5 reveals the existence of two consecutive
423 high-frequency cycles of still-stand and falling stages of wave-base superimposed to
424 the forced regressive stage that took place at the end of third-order Kim-1 sequence
425 (Aurell et al., 1998; Bádenas & Aurell, 2001b). The general downstepping pattern
426 observed in the low angle prograding sub-units indicates a progressive loss of the
427 available accommodation. The siliciclastic dominance at the upper part of units 4 and 5
428 fits with a forced regression context with reduced net carbonate production and
429 increased detrital sediment supply (Catuneanu *et al*., 2011). However, the absence of

significant erosion or evidences of subaereal exposure on top of the downlapping units 4 and 5 reflects that the carbonate ramp was never exposed before the basinwide deepening event that took place at the onset of the Kim-2 sequence deposition (Bádenas & Aurell, 2001a).

High-frequency stages of wave-base oscillations, both linked to variations in the energetic storm conditions (i.e. accretional and erosional stages) and to those related with relative sea-level variations, had a major control on the observed stacking of units 1–5 and their internal sedimentary architecture. The erosive bounding surfaces that appear within these units (i.e. set boundaries, sub-unit boundaries) usually cut the upper part of underlying sets, so topset facies A are frequently reduced or absent. Accordingly, foreset facies B dominates most of the sub-units. The local preservation of topset facies A (mostly in units 2 and 3) can be attributed to stages with high wave-base and more accommodation space compared with units 4 and 5 (Steel & Olsen, 2002, Helland-Hansen & Hampson, 2009). However, in general, accommodation space was limited and the topset area acted as a by-pass area with erosion and/or non-sedimentation (Kohsiek & Terwindt, 1981).

The local preservation of bottomset facies C in the distal part of the units and sub-units is closely related with the occurrence of tangencial wedging (lower part of units 2 and 3). Tangencial wedging architecture with well-developed clinoformed facies distribution A-B-C and distal accumulation of marly and lime mudstone deposits is likely to be favoured during accommodation gain stages (i.e. high wave-base) and/or when sediment supply is low (Mitchum *et al*., 1977, Pomar *et al*., 2015). Otherwise, stages of low wave-base with increased storm intensity and/or higher sediment supply would produce downlap architecture with reduced or absent accumulation of

454 bottomset facies C. It is remarkable to notice that downlap-dominated units in Ricla
455 show higher occurrence of erosive set boundaries and reduced or absent topset facies
456 A, which has been interpreted here as reflecting higher-energy conditions during
457 stages of wave-base fall.
458
459 *6.2. Progradation of units: the shift of the sand-wedge migration*
460 During the Late Jurassic, the carbonate ramp developed in the Iberian Basin was
461 oriented with the deeper domains towards the southeast (Bádenas & Aurell, 2001b).
462 However, palaeocurrent data of the older units (units 1 & 2) recorded at the onset of
463 Ricla Member progradation indicate a southwest direction (Figs. 5 & 10). These values
464 could either be explained by 1) the presence of possible local palaeogeographic
465 irregularities and/or 2) the action of the Ekman effect, so migration would be deflected
466 clockwise with respect to the storm return currents (Warren, 1976). That fits with what
467 is observed in similar Holocene sedimentary bodies at 25-30 m-depth, such as those
468 found in Holocene sediments of the SW and SE Spanish coast, which show oblique
469 sediment transport not directly seawards (Lobo *et al*., 2005; Fernández-Salas et al.,
470 2009). In addition, average palaeocurrent values display an overall southwards
471 migration which progressively shifts from southwest (units 1-2) to southeast (units 3-5)
472 dominant values, indicating a gradual and continuous eastwards deflection of the
473 sand-wedge progradation (Figs. 5 and 10). This progressive deviation against what
474 would be expected by the Ekman Effect, together with the lax arrangement of the
475 most distal units and its foreset angle loss could reflect that successive units were
476 accumulated taking the available accommodation space left by previous units
477 (Posamentier *et al.*, 1988; Posamentier & Allen 1993). The wave-base fall during the

forced regressive stage would accentuate this effect, as it is recorded by greater deflection shown by units 4 and 5. Those architectural implications are less marked in the stacking of Unit 2 over Unit 1, due to an increase of physical accommodation caused by wave-base rise as indicated by the aggrading pattern showed by Unit 2 facies architecture.

6.3. Regional and conceptual implications

The planar cross-stratification dominating the Ricla Member has previously been interpreted as generated by basinward migration of straight-crest bedforms (i.e. dunes) in a sand-shoal complex in shallow conditions near the wave base, controlled by storm return currents (Bádenas & Aurell, 2001a). Further analysis exposed in this work show that sedimentary features in the Ricla Member points to a slightly sloping depositional surface in which topset, foreset and bottomset parts can be recognized, and fit properly with an infralittoral prograding wedge, deposited below the wave base by sediment swept offshore from shallow water environments by wave action (*sensu* Hernandez-Molina *et al.*, 2000). Shallow domains of wave-dominated coasts during sea level highstands usually record stronger currents and higher littoral washing, which can lead to the development of these sedimentary bodies. In addition, the existence of a confined shallow coast, supported by the restricted lateral extension of the Ricla Member would favour the influence of storm-induced currents as it is observed by some authors (e.g. Morton, 2002). The longshore rip currents recorded in the topset part by facies A would supply the sediment from the shallow areas, but the progradation of the Ricla infralittoral prograding wedge was mainly controlled by avalanching processes produced by downwelling storm-induced return currents, since

502 the accretion of cross-beds represent the main horizontal sediment accumulation
503 (Allen, 1968; Kohsiek & Terwindt, 1981; Bádenas & Aurell, 2001a). Observations in
504 modern analogues from the SE Atlantic Spain coast (Gulf of Cádiz) and SW
505 Mediterranean Sea show a <1˚ seafloor morphology and identify a ~3˚ slope break
506 located 20-35 m-depth which coincides with the mean level of storm wave-base
507 (Hernandez-Molina *et al.*, 2000, Fernandez-Salas *et al.*, 2003; Chiocci *et al*., 2004; Lobo
508 *et al.*, 2004, 2005). Figure 11 show the comparison of a part of the Holocene
509 infralittoral prograding wedge in the Gulf of Cádiz (Lobo *et al*., 2005) that allows
510 recognizing their similar sedimentary architecture. Nevertheless, both examples have
511 different nature of sediments and probably time duration. The sedimentary record in
512 those Holocene analogues consists on siliciclastic deposits, not mixed oolitic-siliciclastic
513 nature as shown in Ricla.
514 An infralittoral prograding wedge has been previously described in a southern
515 locality of the Iberian Basin, with a similar stratigraphic position at the upper regressive
516 part of the Kim-1 sequence (i.e., Pozuel Formation, Pomar *et al*., 2015). The dip angle
517 in foreset beds of Pozuel Formation ranges between 5˚ and 10˚, which are similar to
518 10˚ average values recorded in foreset facies B in Ricla, in same range as those
519 observed in Holocene deposits by Lobo *et al*. (2005). However, infralittoral prograding
520 wedges can have a very variable dip of clinobeds (up to 20˚; e.g. Andrieu *et al.*, 2017).
521 As indicated in Fig. 9C, higher angle clinobeds can be recorded in Ricla (up to 15˚).
522 These slightly more inclined cross-bedded beds suggest the presence there of a gentle
523 break-slope, as a result of the inherited topography from the previous foresets, sub-
524 units and units. The inherited topography would favour the development of a more
525 pronounced wedge-shaped deposit, so sets get less inclined in the southern distal

areas as the topography flattens. The internal structure and architecture of Holocene infralittoral prograding wedges in south Spain coast is also complex owing to a lateral accumulation of individual prograding wedges and adaptation to previous deposits (Lobo et al., 2005; Fernández-Salas et al., 2009).

The infralittoral prograding wedge model described by Hernandez-Molina *et al*. (2000) indicates the presence of foreset beds downlapping over finer-grained offshore deposits, and in turn, overlained by shoreface deposits. The Ricla Member, as well as Pozuel Formation (Pomar *et al*., 2015), show a distal interfingered relation of bottomset facies C with marly and lime mudstone distal deposits, corresponding to the offshore domain. As regards to the innermost areas located near the shoreline, the depositional model for Pozuel Fm considers a calm restricted domain with microbial and metazoan mounds developed landwards of the subtidal prograding slope (Pomar *et al*., 2015). In what concerns the Ricla Member, those proximal environments located landwards of the sand-wedge (i.e. upper shoreface and foreshore) remain in doubt, since no shallower deposits are recorded in the exposed areas. This absence could be due to the posterior erosive action. Nonetheless, the top of Ricla Member does not show evidence of subaerial exposure. More likely, it can be explained as resulted by non-deposition stages, as sedimentation was controlled by physical accommodation. The presence of a cemented and ferruginous flat surface in the top of units 2 and 3 could therefore reflect the development of a shallow-water pavement with conditions of sediment by-pass (Purser, 1969), acting as a foreshore area proximally related to the sand-wedge facies.

Infralittoral prograding wedges require a wave-dominated sedimentary environment for developing, which fits with the sedimentary model proposed for the

550 Kimmeridgian ramp by previous regional works (Bádenas & Aurell, 2001a, 2001b).
551 However, modern wave-dominated oolitic systems are not developed as infralittoral
552 prograding wedges but peloid-ooid-skeletal sheets or shoal complexes. Current
553 carbonate production zones, such as those observed in Bahamas (Hine *et al.*, 1981;
554 Rankey *et al.*, 2009; Rankey, 2014) are located in flat platforms which are mostly
555 leewards oriented, controlled by fair weather waves with relatively quieter energy
556 conditions in comparison to those controlling sedimentation in Ricla.
557

558 **7. Conclusions**

559 Three facies types (Facies A, B and C) composed by variable proportion of ooids
560 and siliciclastic detritical grains have been recognized within a progrational wedge-
561 shaped shallow marine unit (Ricla Member, Kimmeridgian, northern Iberian Basin).
562 These three facies are laterally related and organized into sigmoidal-shaped sets,
563 which define a clinoformed depositional model and correspond respectively to the
564 topset, foreset and bottomset parts. The topset part (Facies A) was dominated by the
565 action of bidirectional longshore rip storm-induced currents which swept the sediment
566 together with downwelling currents basinwards. Those currents controlled avalanching
567 processes along the foreset part(Facies B) and defined the main accumulation and
568 seaward prograding migration. The bottomset part (Facies C) was affected by
569 alternating periods of agitation and quiescence, and occasionally oscillatory flows at
570 the toe of the clinoform caused reworking on these distal sediments. All those
571 sedimentological features together support the interpretation of the Ricla Member as
572 an infralittoral prograding wedge.

The significance of these facies heterogeneities and master bedding distribution have been attributed as a sedimentary response to the mixed effect of autogenic (avalanching processes) and allogenic (wave-base oscillations) signal controlling the equilibrium profile during the long-term regressive stage of the Kim-1 sequence.

Five successive units have been identified on the basis of stacking patterns and facies distribution. Those units are internally arranged in sub-units and sets, and reflect the evolutionary stages of the Ricla infralittoral prograding wedge during still-stand and forced regression as well as a progressive deviation in the migration trends which could indicate that each unit was accommodated over the space left by previous ones.

The better knowledge about the Ricla Member infralittoral prograding wedge exposed in this work offers a well-understood continuous outcropping example that can be used to understand other similar grain-supported deposits. As already underlined in Pomar *et al*. (2015), the infralittoral wedge model has a broad potential application to other prograding grain-dominated lithosomes that do not conform to the traditional sand shoal model, being some of them significant hydrocarbon reservoirs.

Acknowledgements

This work has been supported by the project CGL2017-85038-P subsidized by the Spanish Ministry of Science and Innovation, the European Regional Development Fund and the project H54 of the Government of Aragón (*Grupos Consolidados* and *Dirección General de Patrimonio Cultural*). The authors sincerely thank Javier Hernandez-Molina and Bjørn Kåre Bryn the help provided and their valuable suggestions in the

development of the sedimentary model. We are grateful to Ernesto Schwarz and Eugene Rankey, whose useful revisions have notably improved the quality of this paper.

References

Aigner, T. (1985). Storm depositional systems. Dynamic stratigraphy in modern and ancient shallow-marine sequences. *Lecture notes in Earth Sciences* 3. Springer, Berlin, 174pp.

Allen, J. (1968). *Current ripples*. North Holland, Amsterdam.

Allen, G. & Posamentier, H. (1999). *Siliciclastic Sequence Stratigraphy – Concepts and Applications*. Society of Economic Petrologists and Paleontologists, 216pp.

Andrieu, S., Brigaud, B., Barbarand, J., & Lasseur, E. (2017). Linking early diagenesis and sedimentary facies to sequence stratigraphy on a prograding oolitic wedge: The Bathonian of western France (Aquitaine Basin). *Marine and Petroleum Geology*, *81*, 169-195.

Aurell, M., Bádenas, B., Bosence, D. & Waltham, D. (1998). Carbonate production and offshore transport on a Late Jurassic carbonate ramp (Kimmeridgian, Iberian Basin, NE Spain): evidence from outcrops and computer modelling. In: Wright, V. &Burchette, T. (eds). *Carbonate ramps*. Geological Society, London, Special Publications 149, 137-161.

Aurell, M., Robles, S., Bádenas, B., Quesada, S., Rosales, I., Meléndez, G. & García Ramos, J.C. (2003). Transgressive-Regressive Cycles and Jurassic Palaeogeography of Northeast Iberia. *Sedimentary Geology* 162, 239-271.

619 Aurell, M., Bádenas, B., Ipas, J., & Ramajo, J. (2010). Sedimentary evolution of an
620 Upper Jurassic epeiric carbonate ramp, Iberian Basin, NE Spain. In: van Buchem, F.,
621 Gerdes, K., Esteban, M. (Eds.), Reference models of Mesozoic and Cenozoic
622 carbonate systems in Europe and the Middle East – stratigraphy and diagenesis.
623 *Geological Society, London, Special Publications*, *329*(1), 89-111.
624 Bádenas, B. & Aurell, M. (2001a). Proximal – distal facies relationships and
625 sedimentary processes in a storm dominated carbonate ramp (Kimmeridgian,
626 northwest of the Iberian Ranges, Spain). *Sedimentary Geology* 139, 319-340.
627 Bádenas, B. & Aurell, M. (2001b). Kimmeridgian palaeogeography and basin evolution
628 of northeastern Iberia. *Palaeogeography, Palaeoclimatology, Palaeoecology* 168,
629 291-310.
630 Bádenas, B., Aurell, M. & Gröcke, D. (2005). Facies analysis and correlation of high-
631 order sequences in middle-outer ramp successions: variations in exported
632 carbonate on basin-wide $\delta^{13}C_{carb}$ (Kimmeridgian, NE Spain). *Sedimentology* 52,
633 1253-1275.
634 Bádenas, B. & Aurell, M. (2008). Kimmeridgian epeiric sea deposits of northeast Spain:
635 sedimentary dynamics of a storm dominated carbonate ramp. In: Holmden, C.,
636 Pratt, B. (Eds.). *Dynamics of epeiric seas.* Geological Association of Canada, special
637 paper 48, 55-71.
638 Benson, D.J. (1988). Depositional history of the Smackover Formation in Southwest
639 Alabama. *Gulf Coast Association of Geological Societies Transactions* 38, 197-205.
640 Bowman, D., Birkenfeld, H., & Rosen, D. S. (1992). The longshore flow component in
641 low-energy rip channels: the Mediterranean, Israel. *Marine geology*, *108* (3-4), 259-
642 274.

643 Castelle, B., Scott, T., Brander, R. W., & McCarroll, R. J. (2016). Rip current types,
644 circulation and hazard. *Earth-Science Reviews*, *163*, 1-21.
645 Cattaneo, A. & Steel, R. (2003). Transgressive deposits: a review of their variability.
646 *Earth-Science Reviews* 62, 187-228.
647 Catuneanu, O., Galloway, W., Kendall, C., Miall, A., Posamentier, H., Strasser, A. &
648 Tucker, M. (2011). Sequence stratigraphy: methodology and nomenclature.
649 *Newsletters on Stratigraphy* 44/3, 173-245.
650 Chiarella, D., & Longhitano, S. G. (2012). Distinguishing depositional environments in
651 shallow-water mixed, bio-siliciclastic deposits on the basis of the degree of
652 heterolithic segregation (Gelasian, southern Italy). *Journal of Sedimentary*
653 *Research*, *82*(12), 969-990.
654 Chiocci, F. L., D'Angelo, S., & Romagnoli, C. (2004). Atlante dei terrazzi deposizionali
655 sommersi lungo le coste italiane. *Memorie Descrittive della Carta Geologica*
656 *d'Italia*, *58*, 1-194.
657 Dercourt, J., Ricou, L. E., & Vrielynck, B. 1993. *Atlas Tethys Palaeoenvironmental Maps:*
658 *Gauthier-Villars, Paris*, *14*.
659 Driscoll, N. & Karner, G. (1999). Three-dimensional quantitative modelling of clinoform
660 development. *Marine Geology* 154, 383-98.
661 Fernandez-Salas, L. M., Lobo, F. J., Hernandez-Molina, F. J., Somoza, L., Rodero, J., del
662 Río, V. D., & Maldonado, A. (2003). High-resolution architecture of late Holocene
663 highstand prodeltaic deposits from southern Spain: the imprint of high-frequency
664 climatic and relative sea-level changes. *Continental Shelf Research*, *23*(11-13), 1037-
665 1054.

666 Fernandez-Salas, L. M., Dabrio, C. J., Goy, J. L., Díaz del Río, V., Zazo, C., Lobo, F. J.,
667 Sanz, J.L. & Lario, J. (2009). Land–sea correlation between Late Holocene coastal
668 and infralittoral deposits in the SE Iberian Peninsula (Western Mediterranean).
669 *Geomorphology*, 104 (1-2), 4-11.

670 Grötsch, J., Suwaina, O., Ajlani, G., Taher, A., El-Khassawneh, R., Lokier, S., Coy, G., van
671 der Weerd, E., Masalmeh, S. & van Dorp, J. (2003). The Arab Formation in central
672 Abu Dhabi: 3-D reservoir architecture and static and dynamic modelling. *GeoArabia*
673 8, 47-86.

674 Hampson, G. J., & Storms, J. E. (2003). Geomorphological and sequence stratigraphic
675 variability in wave-dominated, shoreface-shelf parasequences. *Sedimentology*, *50*
676 (4), 667-701.

677 Helland-Hansen, W., & Hampson, G. J. (2009). Trajectory analysis: concepts and
678 applications. *Basin Research*, *21*(5), 454-483.

679 Hernandez-Molina, F.J., Fernandez-Salas, L.M., Lobo, F., Somoza, L., Díaz-del-Río, V. &
680 Dias, J.M.A. (2000). The infralittoral prograding wedge: a new large-scale prograding
681 sedimentary body in shallow marine environments. *Geo-Marine Letters* 20, 109-
682 117.

683 Hine, A. C., Wilber, R. J., & Neumann, A. C. (1981). Carbonate sand bodies along
684 contrasting shallow bank margins facing open seaways in northern Bahamas. *AAPG*
685 *bulletin*, *65*(2), 261-290.

686 Hunt, D. & Tucker, M. (1992). Stranded parasequences and the forced regressive
687 wedge systems tract: deposition during base level fall. *Sedimentary Geology* 81, 1-9.

688 Hunt, D. & Tucker, M. (1995). Stranded parasequences and the forced regressive
689 wedge systems tract: deposition during base level fall – reply. *Sedimentary Geology*
690 95. 147-160.
691 Jenkyns, H (1996). Relative sea-level change and carbon isotopes: data from the Upper
692 Jurassic (Oxfordian) of central and Southern Europe. *Terra Nova* 8, 75-85.
693 Kleipool, L., Reijmer, J., Bádenas, B. & Aurell, M. (2015). Variations in petrophysical
694 properties along a mixed siliciclastic carbonate ramp (Upper Jurassic, Ricla, NE
695 Spain). *Marine and Petroleum Geology* 68, 158-177.
696 Kleipool, L., Reijmer, J., Hardebol, N., Bertotti, G., Aurell, M. & Bádenas, B. (2016).
697 Fracture distribution along an Upper Jurassic carbonate ramp, NE Spain. *Marine and*
698 *Petroleum Geology* 70, 201-221.
699 Kohsiek, L. & Terwindt, J. (1981). Characteristics of foreset and topset bedding in
700 megaripples related to hydrodynamic conditions on an intertidal shoal. *Special*
701 *Publications of the International Association of Sedimentology* 5, 27-37.
702 Lobo, F. J., Sánchez, R., González, R., Dias, J. M. A., Hernandez-Molina, F. J., Fernandez-
703 Salas, L. M., Díaz del Rio, V. & Mendes, I. (2004). Contrasting styles of the Holocene
704 highstand sedimentation and sediment dispersal systems in the northern shelf of
705 the Gulf of Cadiz. *Continental Shelf Research*, *24*(4-5), 461-482.
706 Lobo, F. J., Fernandez-Salas, L. M., Hernandez-Molina, F. J., González, R., Dias, J. M. A.,
707 Díaz del Rio, V. & Somoza, L. (2005). Holocene highstand deposits in the Gulf of
708 Cadiz, SW Iberian Peninsula: a high-resolution record of hierarchical environmental
709 changes. *Marine Geology*, 219 (2), 109-131.
710 MacMahan, J. H., Thornton, E. B. & Reniers, A. J. (2006). Rip current review. *Coastal*
711 *Engineering*, *53* (2-3), 191-208.

712 Marsaglia, K. & Klein, G. De V. (1983). The palaeogeography of Paleozoic and Mesozoic
713 storm depositional systems. *Journal of Geology* 91, 117-142.
714 Mitchum Jr, R. M. (1977). Seismic stratigraphy and global changes of sea level. Part 11:
715 glossary of terms used in seismic stratigraphy. In: Payton, C.E. (ed.), *Seismic*
716 *stratigraphy-Applications to Hydrocarbon Exploration*. AAPG, 205-212.
717 Mitchum Jr, R. M., Vail, P. R. & Sangree, J. B. (1977). Seismic stratigraphy and global
718 changes of sea level. Part 6: stratigraphic interpretation of seismic reflection
719 patterns in depositional sequences: Section 2. Application of seismic reflection
720 configuration to stratigraphic interpretation. In: Payton, C.E. (ed.), *Seismic*
721 *stratigraphy-Applications to Hydrocarbon Exploration*. AAPG, 117-133.
722 Morton, R. A. (2002). Factors controlling storm impacts on coastal barriers and
723 beaches: a preliminary basis for near real-time forecasting. *Journal of Coastal*
724 *Research*, 486-501.
725 Myrow, P. & Southard, J. (1996). Tempestite deposition. *Journal of Sedimentary*
726 *Research (SEPM)* Vol. 66, No. 5, 875-887.
727 Olariu, C., Steel, R., Dalrymple, R. & Gingras, M. (2012). Tidal dunes versus tidal bars:
728 The sedimentological and architectural characteristics o compound dunes in a tidal
729 seaway, the lower Baronia Sandstone (Lower Eocene), Ager Basin, Spain.
730 *Sedimentary Geology* 279, 134-155.
731 Osete, M.L., Gómez, J.J., Pavón-Carrasco, F.J., Villalaín, J.J., Palencia-Ortas, A., Ruiz-
732 Martínez, V.C. & Heller, F. (2011). The evolution of Iberia during the Jurassic from
733 palaeomagnetic data. *Tectonophysics* 502, 105-120.

734 Pomar, L. & Tropeano, M. (2001). The Calcarenite di Gravina Formation in Matera
735 (southern Italy): new insights for coarse-grained, large-scale, cross-bedded bodies
736 encased in offshore deposits. *AAPG bulletin* 85 (4), 661-689.
737 Pomar, L. & Kendall, C. (2008). Architecture of carbonate platforms: a response to
738 hydrodynamics and evolving ecology. In: Lukasik, J., Simo, A. (Eds.), Controls on
739 Carbonate Platform and Reef Development, SEPM Spec. Public, vol. 89, 187-216.
740 Pomar, L., Aurell, M., Bádenas, B., Morsilli, M. & Al-Awwad, S.F. (2015). Depositional
741 model for a prograding oolitic wedge, Upper Jurassic, Iberian Basin. *Marine and*
742 *Petroleum Geology* 67, 556-582.
743 Posamentier, H. W., Jervey, M. T., & Vail, P. R. (1988). Eustatic controls on clastic
744 deposition I—conceptual framework.
745 Posamentier, H. W., & Allen, G. P. (1993). Variability of the sequence stratigraphic
746 model: effects of local basin factors. *Sedimentary geology*, *86*(1-2), 91-109.
747 Price, G., Sellwood, B. & Valdes, P. (1995). Sedimentological evaluation of general
748 circulation model simulations for the “greenhouse” Earth: Cretaceous and Jurassic
749 case studies. *Sedimentary Geology* 100, 159-180.
750 Puig. P., Ogston, A., Guillén, J., Fain, A. & Palanques, A. (2007). Sediment transport
751 processes from the topset to the foreset of a crenulated clinoform (Adriatic Sea).
752 *Continental Shelf Research* 27, 452-474.
753 Purser, B. H. (1969). Syn-sedimentary marine lithification of Middle Jurassic limestones
754 in the Paris Basin. *Sedimentology*, *12*(3-4), 205-230.
755 Rankey, E. C., Guidry, S. A., Reeder, S. L., & Guarin, H. (2009). Geomorphic and
756 sedimentologic heterogeneity along a Holocene shelf margin: Caicos
757 Platform. *Journal of Sedimentary Research*, *79*(6), 440-456.

758 Rankey, E. C., & Reeder, S. L. (2011). Holocene oolitic marine sand complexes of the
759 Bahamas. *Journal of Sedimentary Research*, *81*(2), 97-117.
760 Rankey, E. C. (2014). Contrasts between wave-and tide-dominated oolitic systems:
761 Holocene of Crooked–Acklins Platform, southern Bahamas. *Facies*, *60*(2), 405-428.
762 Rich, J. (1951). Three critical environments of deposition and criteria for recognition of
763 rocks deposited in each of them. *Geological Society of American Bulletin* 62, 1-20.
764 San Miguel, G., Aurell, M., Bádenas, B., Martínez, V., Caline, B., Pabian-Goyheneche, C.,
765 Rolando, J.P. & Grasseau, N. (2013). Facies heterogeneity of a Kimmeridgian
766 Carbonate Ramp (Jabaloyas, Eastern Spain): a combined outcrop and 3D
767 geomodelling analysis. *Journal of Iberian Geology* 39: 233-252.
768 Schlager, W. (2005). *Carbonate sedimentology and sequence stratigraphy* (No. 8).
769 SEPM Society for Sedimentary Geology.
770 Steel, R. J., & Olsen, T. (2002). Clinoforms, clinoform trajectories and deepwater sands.
771 In *Sequence-stratigraphic models for exploration and production: Evolving*
772 *methodology, emerging models and application histories: Gulf Coast Section SEPM*
773 *22nd Research Conference, Houston, Texas* (pp. 367-381).
774 Storms, J. E., & Hampson, G. J. (2005). Mechanisms for forming discontinuity surfaces
775 within shoreface–shelf parasequences: sea level, sediment supply, or wave
776 regime?. *Journal of Sedimentary Research*, *75*(1), 67-81.
777 Strasser, A. (1986). Ooids in Purbeck limestones (Lowermost Cretaceous) of the Swiss
778 and French Jura. *Sedimentology* 33, 711-727.
779 Swift, D. (1968). Coastal erosion and transgressive stratigraphy. The Journal of Geology
780 76, 444-456.

781 Taylor, A.M. & Goldring, R. (1993). Description and analysis of bioturbation and
782 ichnofabric. *Journal of the Geological Society of London* 150, 141-148.
783 Tucker, M. & Wright, V. (1990). *Carbonate Sedimentology*. Blackwell, London, 482pp.
784 Tucker, M. (1985). Shallow-marine carbonate facies and facies models. *Geological*
785 *Society, London, Special Publications* 18, 147-169.
786 Walsh, J., Nittrouer, C., Palinkas, C., Ogston, A., Sternberg, R. & Brunskill, G. (2004).
787 Clinoform mechanics in the Gulf of Papua, New Guinea. *Continental Shelf Research*
788 24, 2487-2510.
789 Warren, A. (1976). Dune trend and the Ekman Spiral. *Nature*, *259*, 653-654.
790 Westphal, H., Halfar, J. & Freiwald, A. (2010). Heterozoan carbonates in subtropical to
791 tropical settings in the present and past. *International Journal of Earth Sciences* 99,
792 153-169.
793 Wright, V. & Faulkner, T. (1990). Sediment dynamics of Early Carboniferous ramps: a
794 proposal. *Geological Journal* 25, 139-144.
795

796 **Figure Captions**

797

798 Figure 1: A): Palaeogeographical context of the Iberian Basin in Western Europe
799 during Kimmeridgian (modified from Dercourt *et al*., 1993; palaeolatitude adapted
800 from Osete *et al*., 2011). B): Geographic location of the studied Kimmeridgian Ricla
801 outcrops within the main Iberian Basin facies belts (modified from Bádenas & Aurell,
802 2012). C): Synthetic chronostratigraphic distribution of the Kimmeridgian facies in the
803 northern Iberian Basin, including the span of the transgressive-regressive Kim-1 and
804 Kim-2 sequences (modified from Aurell *et al*., 2010). The bold box indicates the

805 stratigraphic location of the studied Ricla Member within the regressive stage of Kim-1
806 sequence. D): General previous data of the Ricla Member lithofacies distribution
807 according to Bádenas & Aurell (2001a). The bold box indicates the range studied here
808 in detail.
809
810 Figure 2: A): Aerial view and distribution of the uppermost Kimmeridgian Ricla
811 Member outcrops (modified from Bádenas & Aurell, 2001a). The location of the ten
812 panoramic outcrop views selected to study is also indicated and they are named. B):
813 Reconstruction of the Ricla Member sedimentary architecture consistent on five
814 prograding units, by the correlation of 10 selected panoramic outcrops, in which the
815 facies distribution and sharp bounding surfaces have been mapped. The basal sand-
816 dominated unit has been considered as a previous detrital episode and is used here as
817 a datum.
818
819 Figure 3: Field view of the different facies identified for the uppermost
820 Kimmeridgian Ricla Member. A): Facies A (topset: bidirectional dm-thick cross-bedded
821 sets). B): Facies B (foreset: unidirectional m-thick planar cross-bedded sets). C): Facies
822 C (bottomset: unidirectional cross-laminated beds with hummocky cross stratification).
823 D): Facies D (tabular bed of poorly sorted sandstone to micro-conglomerate).
824
825 Figure 4: Thin-section images in petrographic microscope with plane-polarized
826 light of the different lithofacies composing the Ricla Member deposits. A): oolitic
827 grainstone. B): oolitic-sandy grainstone. C): oolitic sandstone in proximal localities. D-
828 E): oolitic sandstone in distal localities. F): heterometric micro-conglomerate.

Figure 5: Distribution of palaeocurrent data taken from different measuring stations along the Ricla Member, indicating its belonging to the five successive units. The dot line marks the inferred minimum extension of each prograding unit front, together with its mean palaeocurrent trend.

Figure 6: Panoramic view of the outcrop 1, which includes Unit 1 and the lower part of Unit 2, its facies distribution and architecture are indicated. Unit 1 shows a lower part with distal facies C and an upper part formed by offlap stacked sub-units with sets dominated by facies B. Unit 2 in outcrop 1 is located over a facies D bed and is composed by offlapping sub-units with sets encompassing facies A, B and C, locally showing down-slope shingling configuration. The boxes A, B and C represent detailed windows focusing close into the outcrop.

Figure 7: Panoramic view of the outcrop 2, which includes the upper part of Unit 2, its facies distribution and architecture are indicated. Unit 2 in outcrop 2 shows downlap architecture and is exclusively formed by facies B arranged in down-slope shingling stacking to offlap stacking sub-units. The boxes A, B and C represent detailed windows focusing close into the outcrop.

Figure 8: Panoramic view of the outcrop 6, which includes Units 4 and 5, its architecture and the distribution of oolitic- and siliciclastic-dominated intervals are indicated. Units 4 and 5 show downstepping architecture, and are formed by

852 offlapping sub-units dominated by facies B with detrital increasing to the top. The
853 boxes A and B represent detailed windows focusing close into the outcrop.
854
855 Figure 9: A): Outcrop window extracted from outcrop 1, which shows the A-B-C
856 facies sigmoidal lateral relationship as it is displayed in the outcrops. B): Sedimentary
857 model proposed for the uppermost Kimmeridgian Ricla Member in the Iberian Basin,
858 consistent in a clinoformed gentle slope with differentiated topset, foreset and
859 bottomset parts, the main sedimentary structures and dominant palaeocurrents in
860 each part are also indicated. C): Depositional evolutionary model of the Ricla
861 infralittoral prograding wedge throughout successive stages of avalanching and wave
862 oscillation. Slope dip angle of the foreset beds varies in accordance to the physical
863 accommodation.
864
865 Figure 10: Evolutionary reconstruction of the Ricla Member building up and
866 interpretation of the high-frequency wave-base oscillations superimposed to the
867 regressive stage of the third-order Kim-1 T-R sequence, controlling the facies
868 distribution and sedimentary architecture of each unit within the Ricla Member. The
869 facies mapping and mean palaeocurrent data for each unit are also indicated.
870
871 Figure 11: comparison of the sedimentary architecture shown by the Ricla
872 Member in this work and an extract of the seismic stratigraphy interpretation of a
873 Holocene infralittoral prograding wedge in the Gulf of Cádiz (Lobo et al., 2005). It has
874 been redrawn form their Fig. 8B to the same scale as the Ricla example.

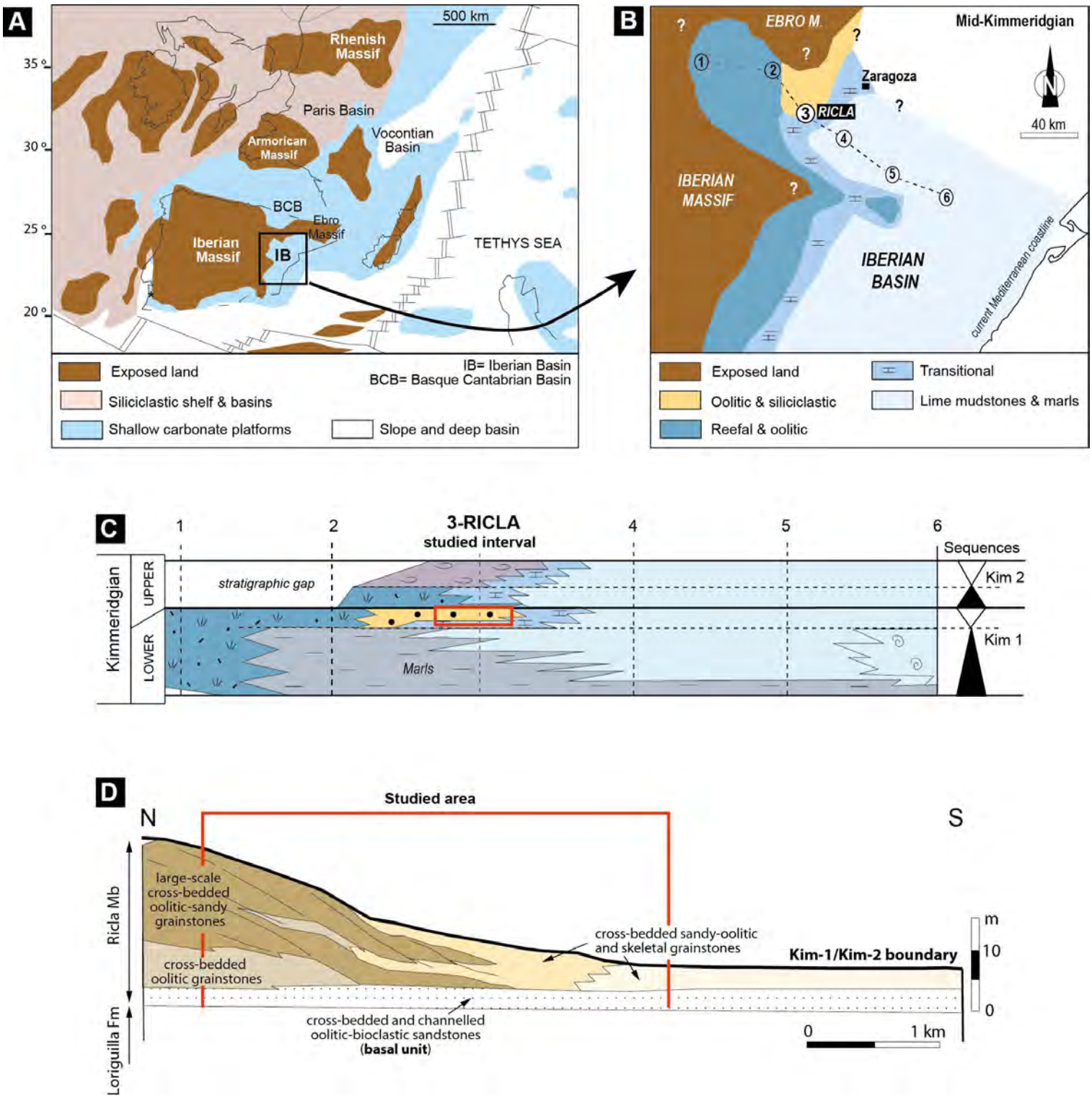
A
500 km
35 °
30 °
25 °
20 °
Rhenish Massif
Paris Basin
Armorican Massif
Vocontian Basin
BCB
Ebro Massif
Iberian Massif
IB
TETHYS SEA
Exposed land
Siliciclastic shelf & basins
Shallow carbonate platforms
Slope and deep basin
IB= Iberian Basin
BCB= Basque Cantabrian Basin
B
EBRO M.
Mid-Kimmeridgian
Zaragoza
RICLA
40 km
IBERIAN MASSIF
IBERIAN BASIN
current Mediterranean coastline
Exposed land
Oolitic & siliciclastic
Reefal & oolitic
Transitional
Lime mudstones & marls
C
3-RICLA
studied interval
Sequences
Kim 2
Kim 1
Kimmeridgian
UPPER
LOWER
stratigraphic gap
Marls
D
Studied area
N
S
Rica Mb
Loriguilla Fm
large-scale cross-bedded oolitic-sandy grainstones
cross-bedded oolitic grainstones
cross-bedded and channelled oolitic-bioclastic sandstones (basal unit)
cross-bedded sandy-oolitic and skeletal grainstones
Kim-1/Kim-2 boundary
m
10
0
0
1 km

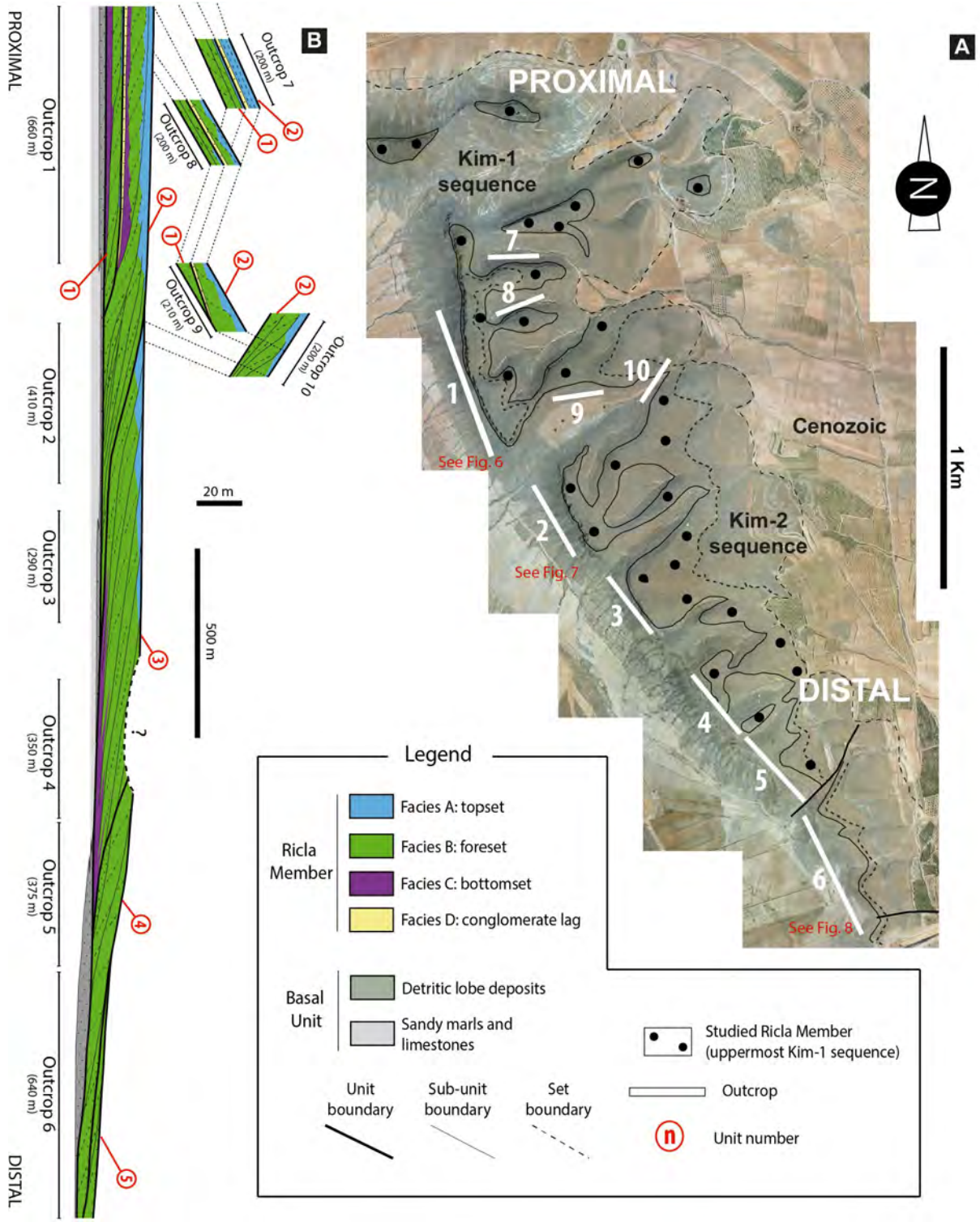
A
B
PROXIMAL
DISTAL
Kim-1 sequence
Kim-2 sequence
Cenozoic
See Fig. 6
See Fig. 7
See Fig. 8
1 Km
N
20 m
500 m
Outcrop 1 (660 m)
Outcrop 2 (410 m)
Outcrop 3 (290 m)
Outcrop 4 (350 m)
Outcrop 5 (375 m)
Outcrop 6 (640 m)
Outcrop 7 (200 m)
Outcrop 8 (200 m)
Outcrop 9 (210 m)
Outcrop 10 (200 m)
Legend
Ricla Member
Facies A: topset
Facies B: foreset
Facies C: bottomset
Facies D: conglomerate lag
Basal Unit
Detritic lobe deposits
Sandy marls and limestones
Studied Ricla Member (uppermost Kim-1 sequence)
Unit boundary
Sub-unit boundary
Set boundary
Outcrop
Unit number


A
B
1 m
C
D

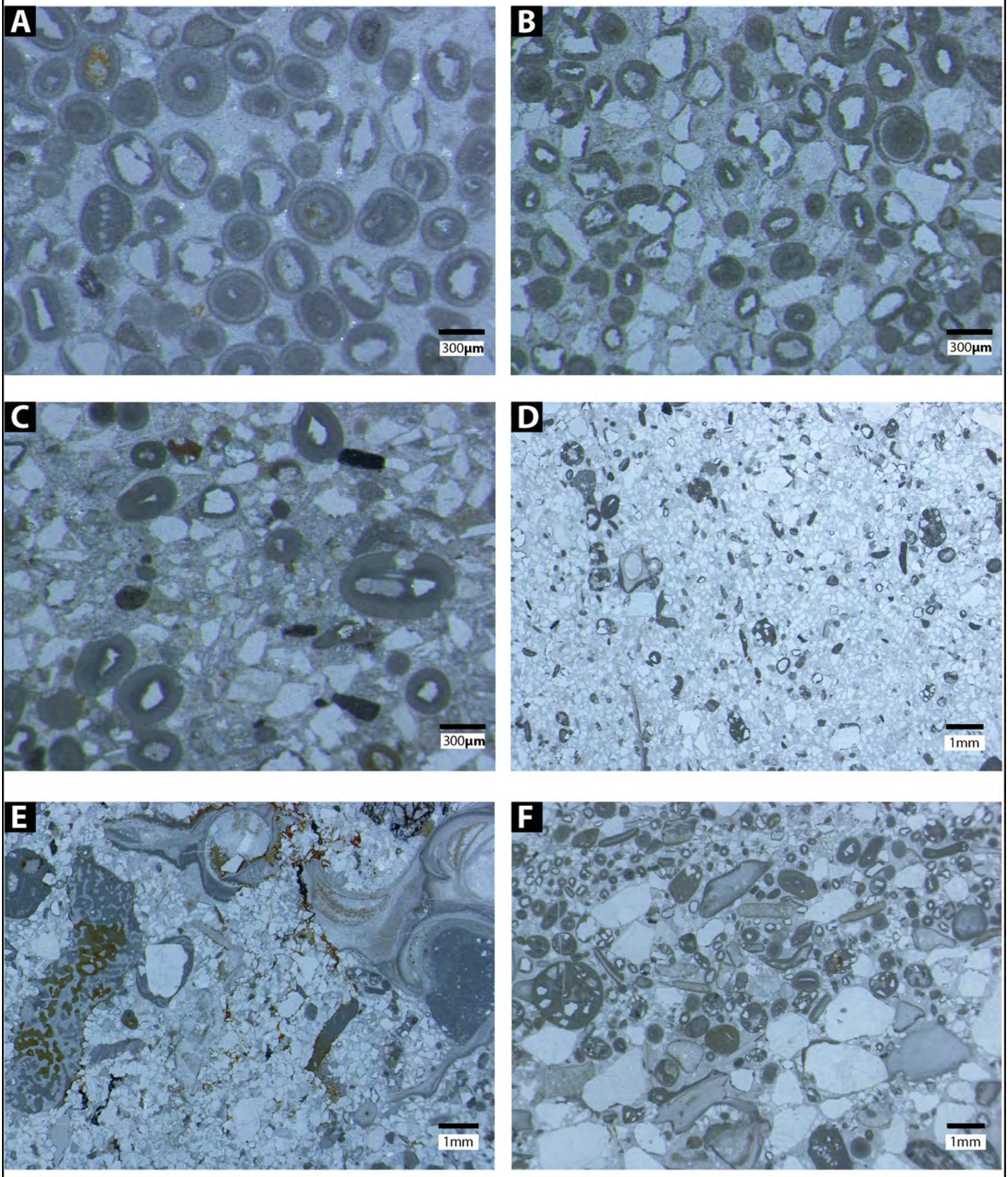
A
300µm
B
300µm
C
300µm
D
1mm
E
1mm
F
1mm

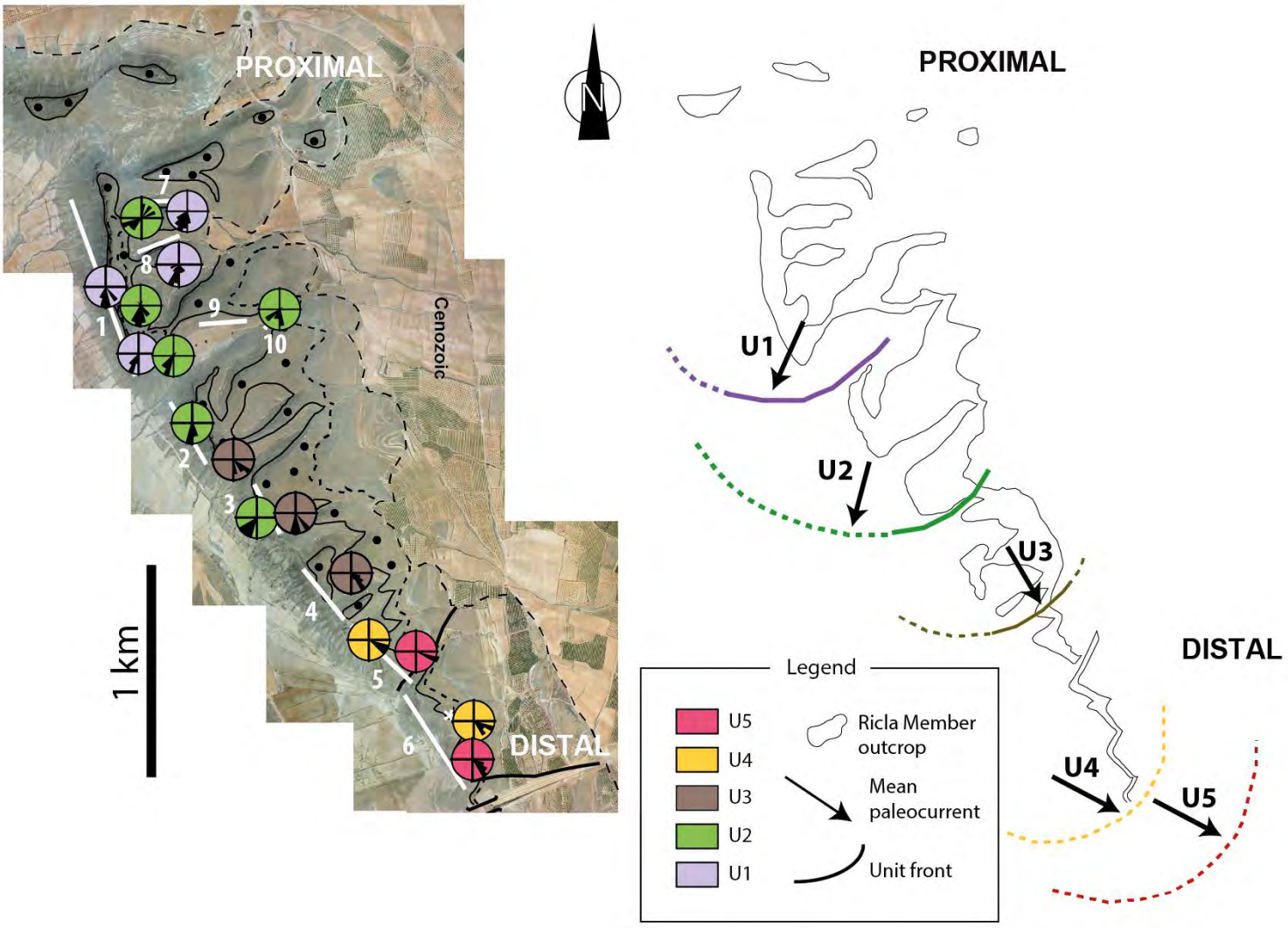
PROXIMAL
Cenozoic
DISTAL
1 km
1
2
3
4
5
6
7
8
9
10
N
PROXIMAL
U1
U2
U3
U4
U5
DISTAL
Legend
U5
U4
U3
U2
U1
Ricla Member outcrop
Mean paleocurrent
Unit front

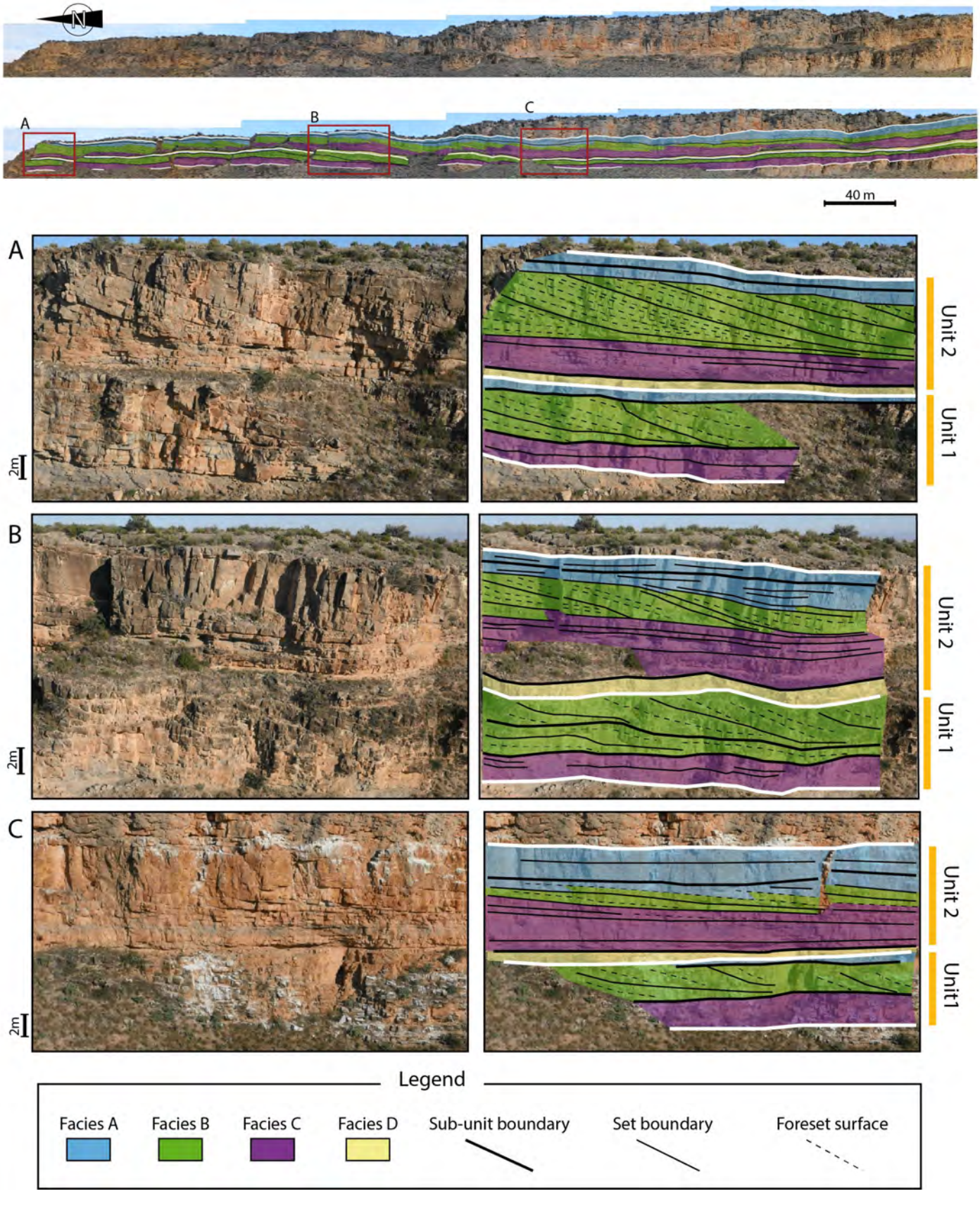
N
A
B
C
40 m
A
2m
Unit 2
Unit 1
B
2m
Unit 2
Unit 1
C
2m
Unit 2
Unit1
Legend
Facies A
Facies B
Facies C
Facies D
Sub-unit boundary
Set boundary
Foreset surface

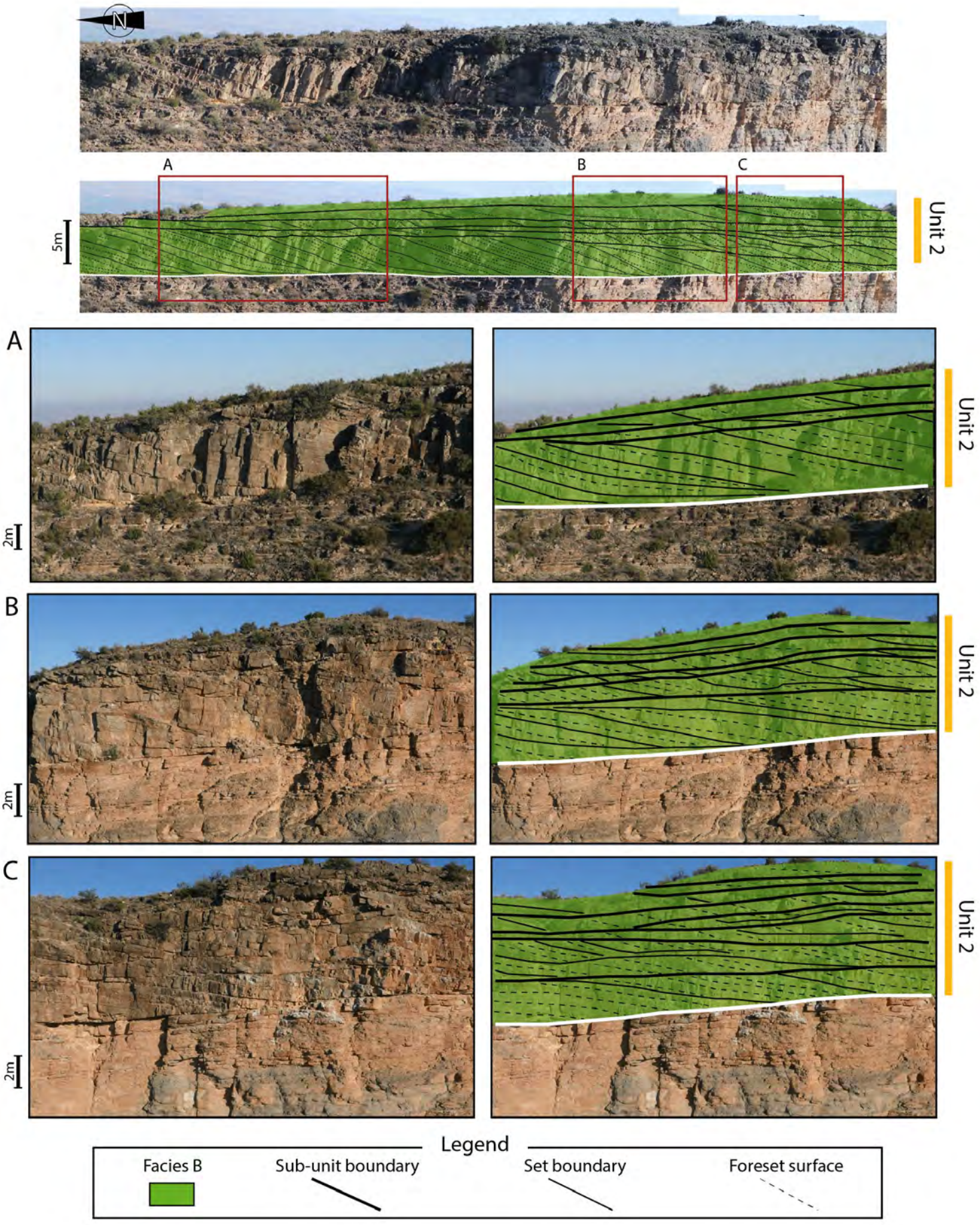
N
A
B
C
5m
Unit 2
A
2m
Unit 2
B
2m
Unit 2
C
2m
Unit 2
Legend
Facies B
Sub-unit boundary
Set boundary
Foreset surface

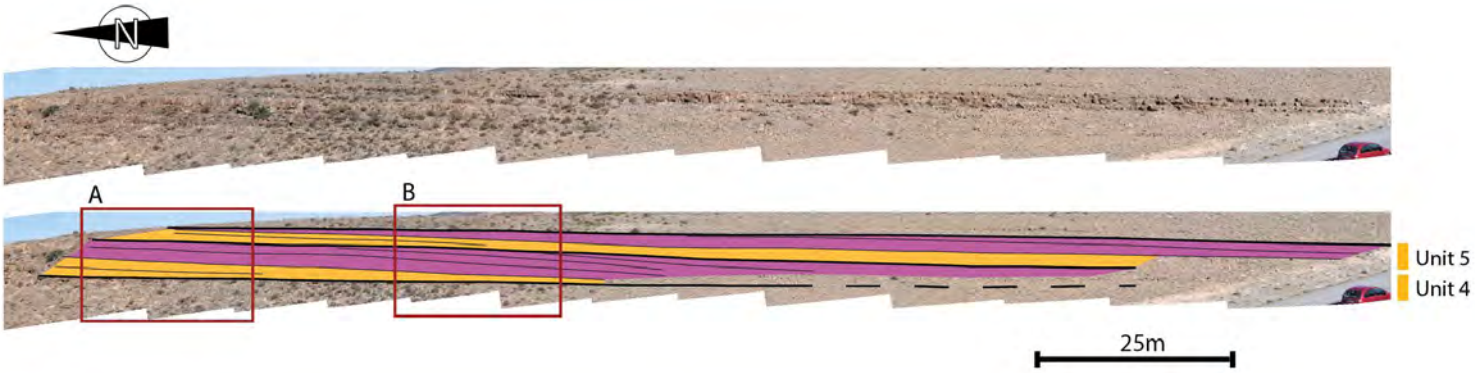
N
A
B
Unit 5
Unit 4
25m

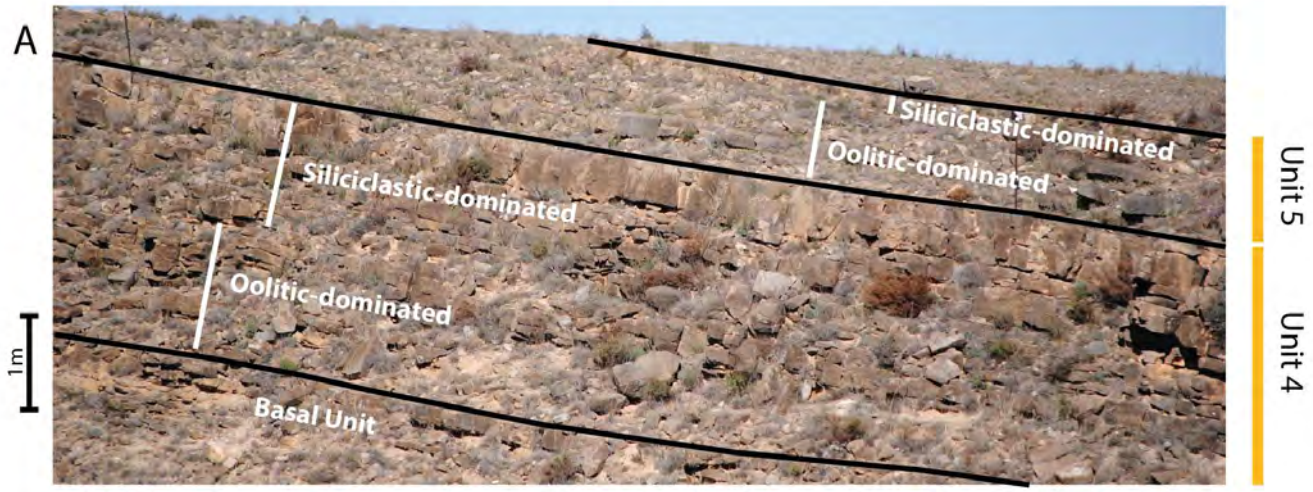
A
Siliciclastic-dominated
Oolitic-dominated
Siliciclastic-dominated
Oolitic-dominated
Basal Unit
1m
Unit 5
Unit 4

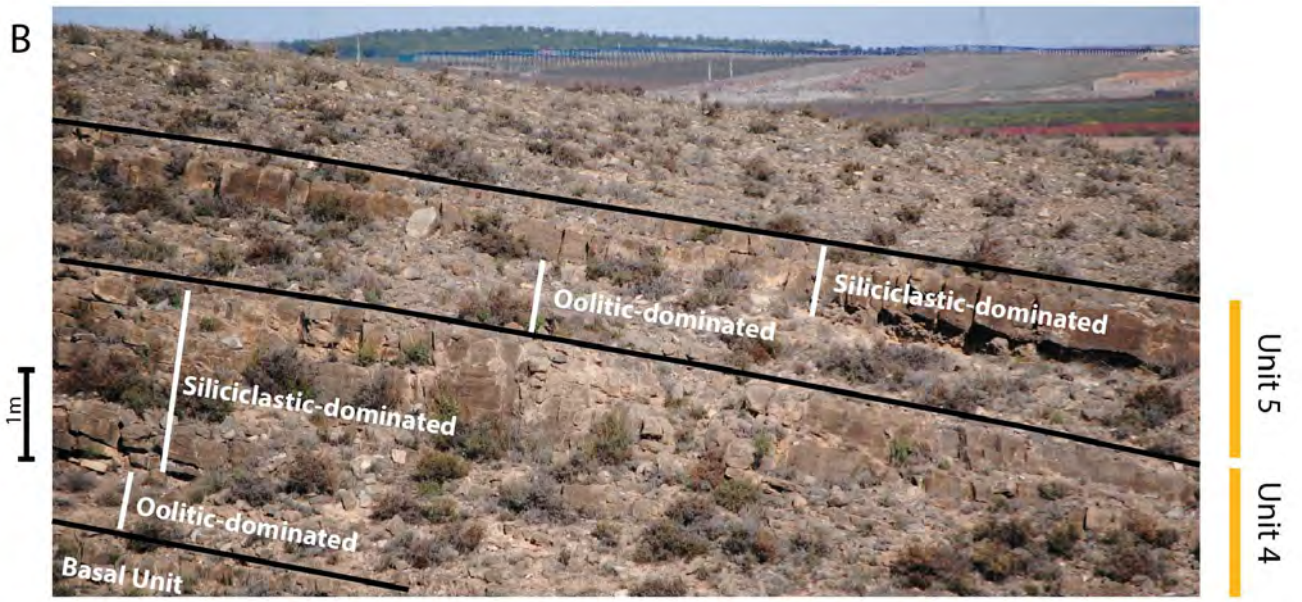
B
Oolitic-dominated
Siliciclastic-dominated
Siliciclastic-dominated
Oolitic-dominated
Basal Unit
1m
Unit 5
Unit 4

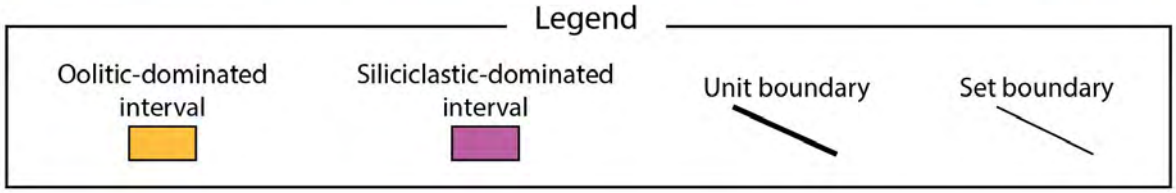
Legend
Oolitic-dominated interval
Siliciclastic-dominated interval
Unit boundary
Set boundary

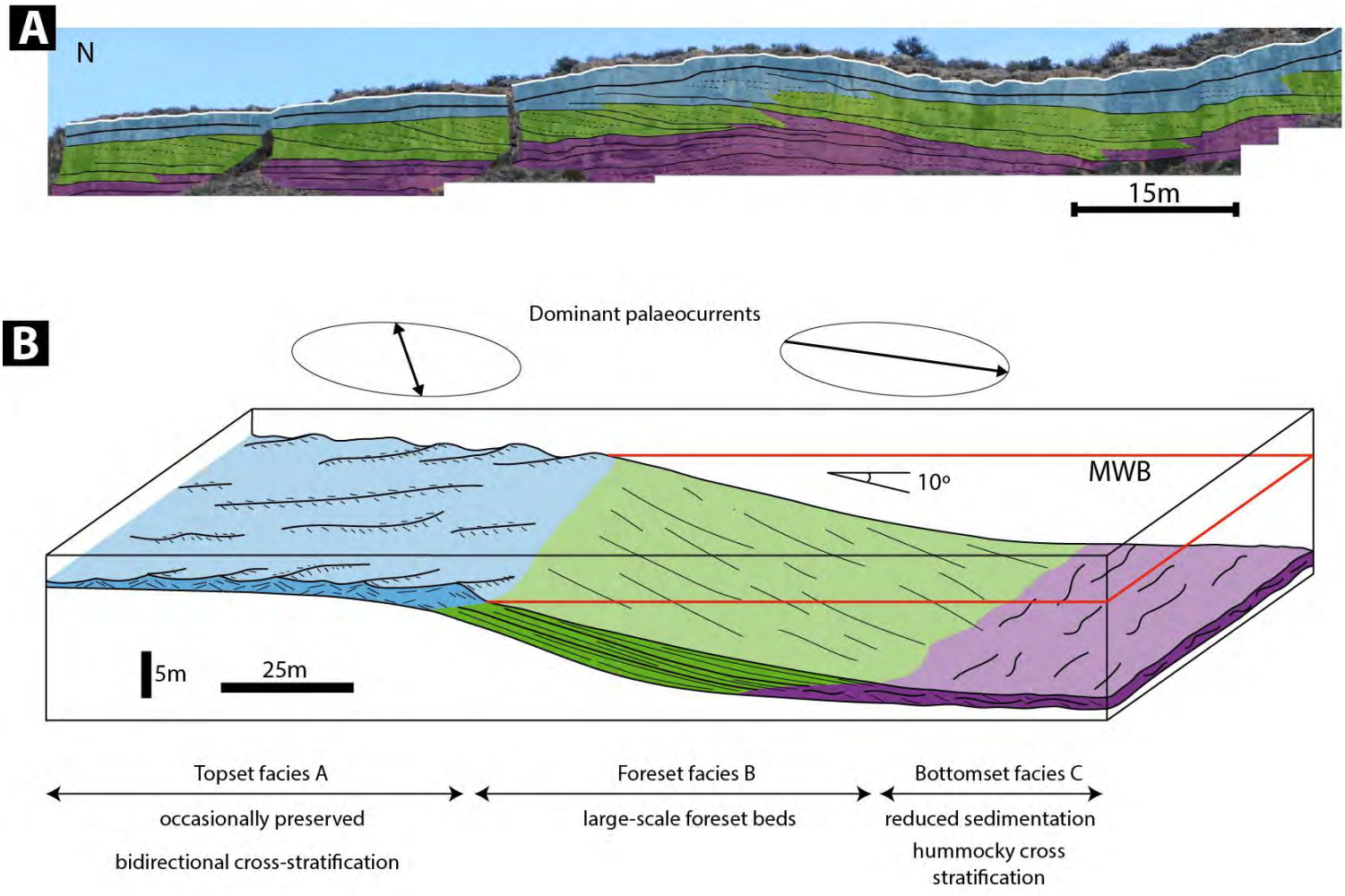
A
N
15m
B
Dominant palaeocurrents
10°
MWB
5m
25m
Topset facies A
occasionally preserved
bidirectional cross-stratification
Foreset facies B
large-scale foreset beds
Bottomset facies C
reduced sedimentation
hummocky cross stratification
C
3
avalanching 3
2
avalanching 2
1
avalanching 1

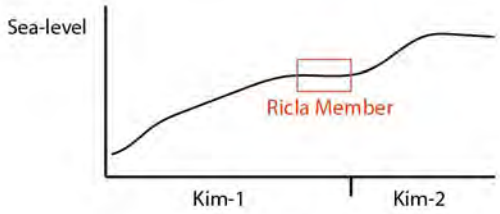

Taken from Aurell et al. (1998)

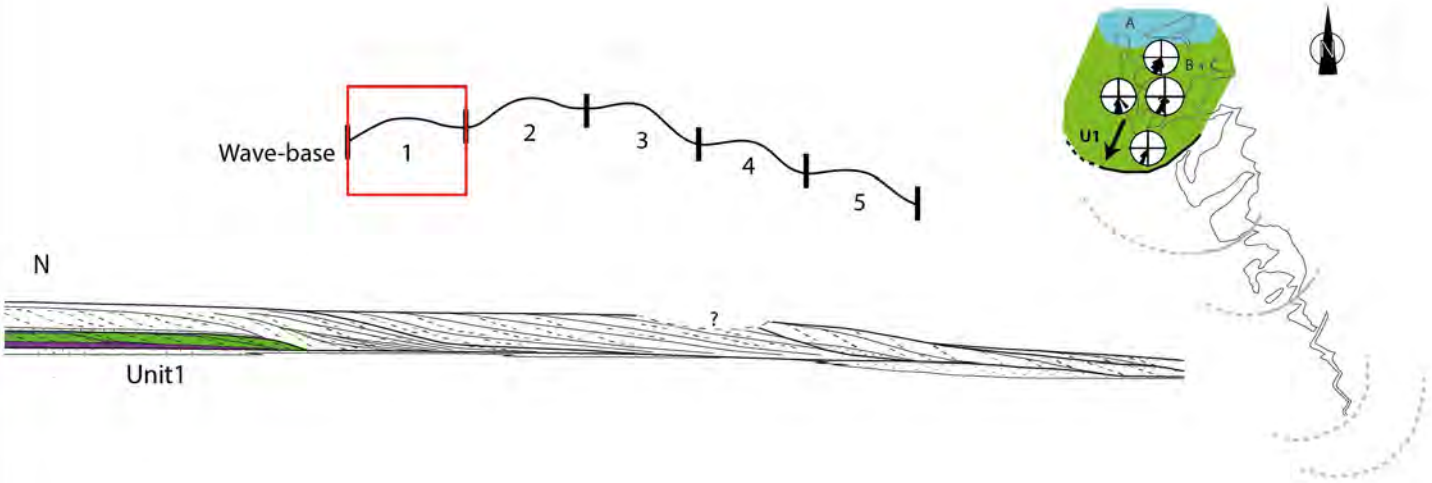

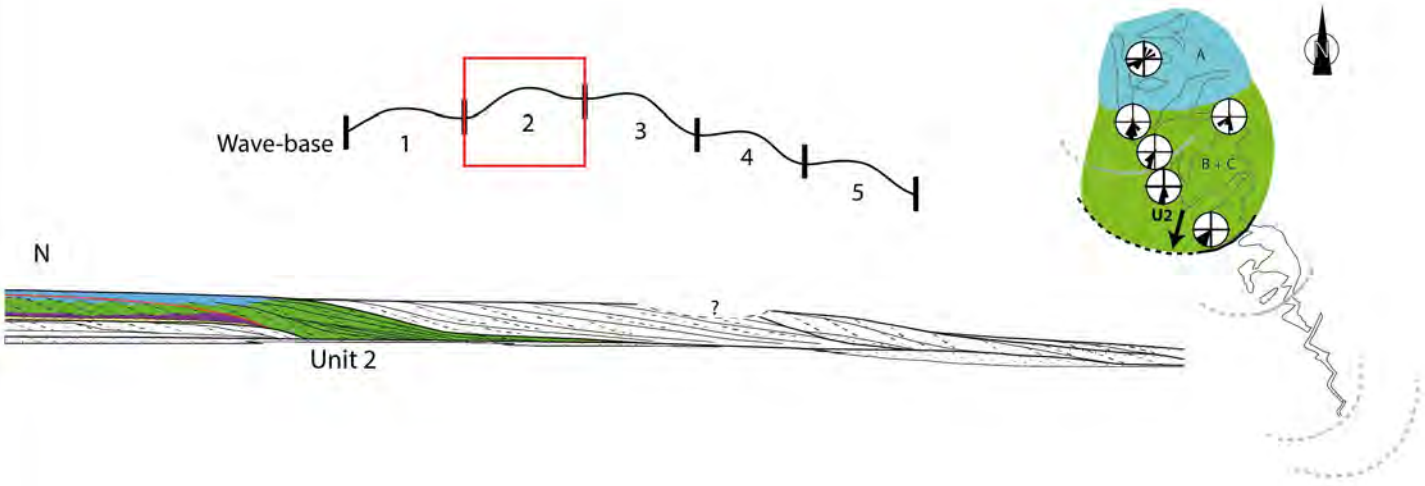

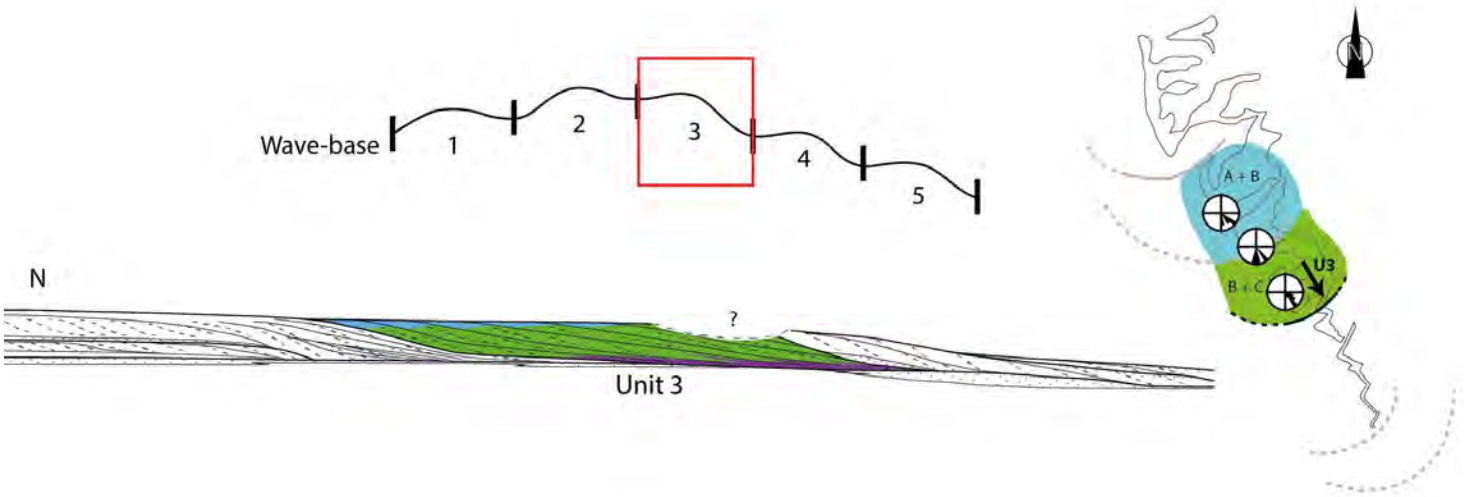
Wave-base
1
2
3
4
5
N
?
Unit 3
N
A + B
B + C
U3

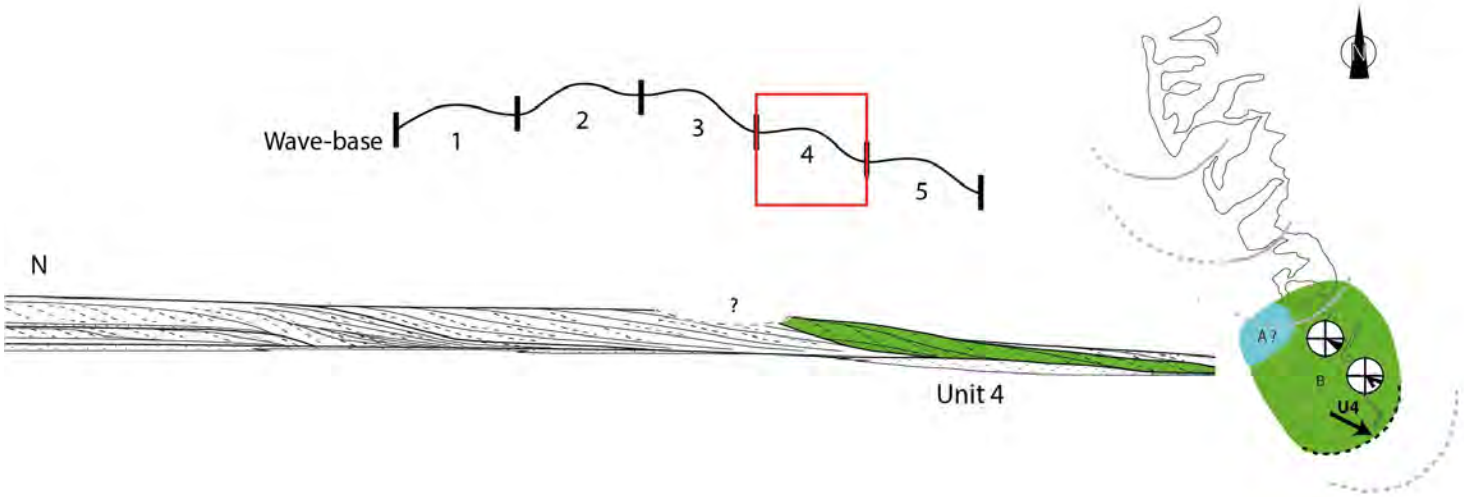
Wave-base
1
2
3
4
5
N
?
Unit 4
N
A ?
B
U4

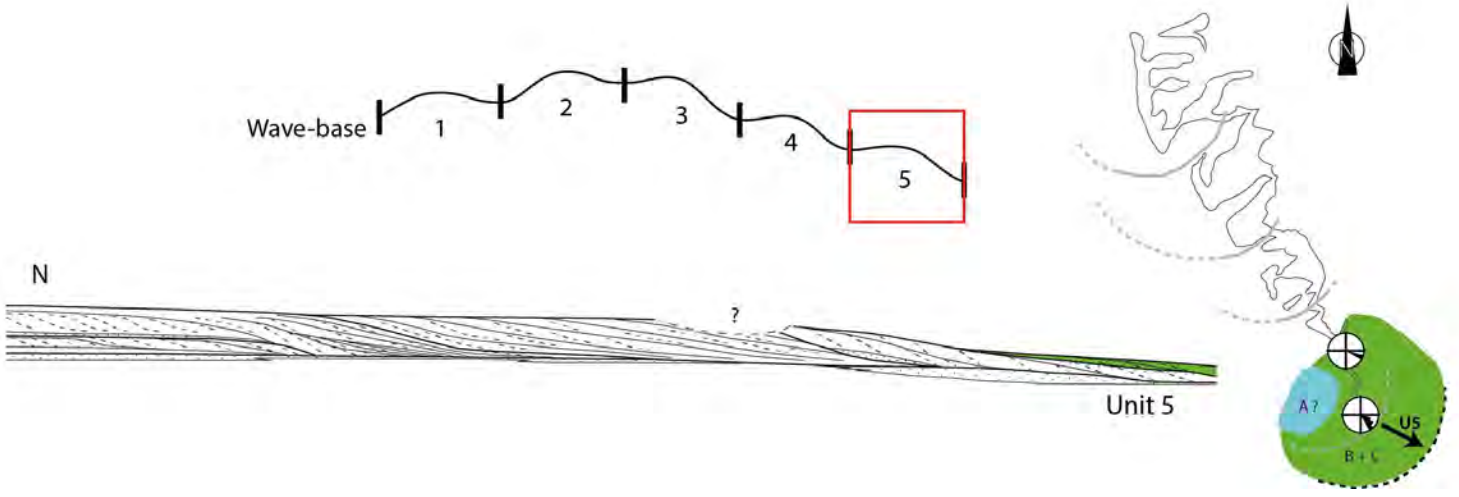
Wave-base
1
2
3
4
5
N
?
Unit 5
N
A ?
B + C
U5

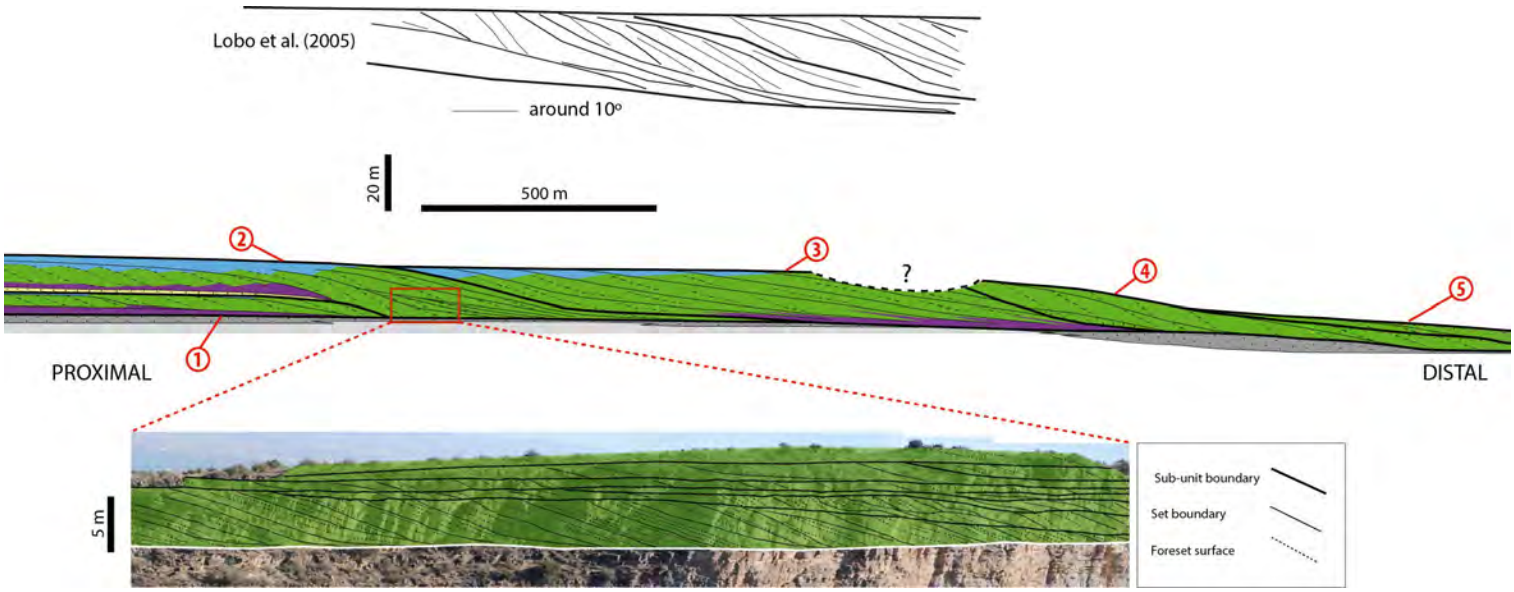
Lobo et al. (2005)
around 10º
20 m
500 m
?
PROXIMAL
DISTAL
5 m
Sub-unit boundary
Set boundary
Foreset surface